JOURNAL OF MATERIALS SCIENCE 26 (1991) 3125–3153

Fabrication and characterization of thin films with perpendicular magnetic anisotropy for high-density magnetic recording

Part II *A review*

C. W. CHEN
Chemistry & Materials Science Department, Lawrence Livermore National Laboratory, University of California, Livermore, CA 94550, USA

Perpendicular magnetic anisotropy (PMA) was first observed in thin films of cobalt–chromium alloys in 1974, and perpendicular magnetic recording was proposed in 1977. After less than ten years, a new technology for high-density magnetic recording is firmly established. This breakthrough of the science and technology of magnetic recording has been made possible mainly through the ingenuity and concerted efforts of Iwasaki and other researchers. The preparation, characterization, and application of the Co–Cr films featuring PMA have been extensively studied. This paper reviews the large number of reports on PMA films with emphasis in three areas: (1) processing of PMA films; (2) correlation of magnetic properties and microstructures of PMA films; and (3) state-of-the-art techniques for fabricating PMA films.

Nomenclature

PMA	Perpendicular magnetic anisotropy
PMR	Perpendicular magnetic recording
B	Magnetic induction
H	Magnetic field
H_c	Coercivity
$H_{c,\perp}$	Perpendicular coercivity
H_d	Demagnetizing field
H_K	Anisotropy field
$H_\perp$	Perpendicular anisotropy constant
M_r	Remanent magnetization
M_s	Saturation magnetization
P_{Ar}	Argon pressure
T_s	Substrate temperature
V_b	Substrate bias voltage
α	Incidence angle
$\Delta\theta_{50}$	Half-width dispersion angle in the rocking curve
θ_c	Curie temperature
σ_o	Internal stress

1. Characterization of PMA films

1.1. Magnetic properties

Magnetic characterization constitutes the principal interest of most ($\sim$ 60%) of the numerous studies of PMA films. The voluminous literature makes it impossible to include in this section every report of magnetic studies. What we shall do is review papers that have contributed importantly to the evaluation or understanding of the dependence of magnetic properties on the microstructure of Co–Cr films. To focus our discussion further, we shall be concerned only with single layers of Co–Cr alloys. Work on double layers, multiple layers, and metallic underlayers will be discussed in Section 2.

Before reviewing the results of selected studies, it will be useful to discuss briefly a few advanced techniques that were applied to studying the magnetic behaviour of PMA films.

Haines developed a new analytical method for performing accurate (within 1%) and repeatable measurements of magnetization–hysteresis (M–H) loop variation with sample thickness [1]. An innovative feature of the method was the computer control of the vibrating-sample magnetometer (VSM) measurements, which incorporated two techniques (VSM depth profiling and differential VS magnetometry, DVSM, measurements) and allowed magnetic properties to be measured as a function of film depth. The profiling was made possible by removing layers of the film by chemical or physical etching after VSM measurements had been made in a point-to-point mode. The loops were stored in computer memory for later uses.

Although VSM profiling leads directly to plots of a given magnetic parameter against increasing depth from the final surface, the DVSM technique subtracts adjacent loops to determine the contribution of a fixed layer to the magnetic properties of the film. This new method is claimed to be a powerful tool for understanding the magnetic behaviour of the PMA films as a function of film thickness. For example, it enables Haines [1] to conclude that, although the hysteresis loop of the film improves as film thickness is increased,

0022–2461/91 $03.00 + .12

the key to optimizing the PMR performance of a Co–Cr medium is control of the structure and magnetic properties of the initial growing layer.

Ferromagnetic resonance (FMR) is a dynamic technique that can distinguish magnetization and anisotropy in various regions by changing the applied field. Mitchell *et al.* [2, 3] have shown that FMR is useful in studying magnetic morphology in Co–Cr films. Their studies led them to believe that each alloy film may be modelled as two elemental layers of the constituent atoms stacking together. Later in the study, they refined the model by adding a transition layer ($\sim$ 96 nm thick with negative effective anisotropy) at the interface of the substrate and the bulk of the film. Ramakrishna *et al.* [4] applied the refined model to assessing the FMR behaviour of a large number of films by varying the thickness of either the Co or the Cr layer while holding the other layer constant. This enabled the latter workers to sort out different magnetic phenomena. To make the study more complete, they also conducted static magnetization measurements based on a SQUID magnetometer. The combined results led them to conclude that there may be long-range magnetic effects giving rise to additional anisotropy fields.

In another resonance study, Cofield *et al.* [5] obtained spin-wave resonance (SWR) spectra from Co–20% Cr thin films deposited on silicon or glass substrates at 298 K on conventional microwave magnetic resonance spectrometers operating at 9.8 and 35.2 GHz at room temperature. The observed spectra enabled them to (a) deduce the value for the exchange constant A to be 1.0×10^{-6} erg cm^{-1}, (b) detect the presence of other magnetic elements in the films showing deviating magnetic behaviour in the SWR spectra, and (c) reveal different magnetic properties of the silicon and glass substrates, from which they inferred a pronounced effect of the substrate on the pinning condition and stress anisotropy field.

Yoshida *et al.* [6] demonstrated that electron holography offers outstanding features for observing magnetic flux in submicrometre regions and for quantitative measurements on the flux intensity in Co–Cr films. Later, they applied the technique to PMR media using a ring-type head for measurements on the intensity of recorded magnetization [7]. The intensity was determined at 200 $\pm$ 20 kA/m, which is three times the remanence measured by a VSM. This vast difference signifies the great reduction of the demagnetizing factor by the presence of stripe domains in the Co–Cr film under perpendicular recording conditions.

Another technique involved the use by Indeck and Judy [8] of a vertical magnetoresistive transducer (MRT) in the read head and a hybrid single-pole-type write head to perform quasi-static measurements. The MRT can differentiate the apparent longitudinal component from the perpendicular component of the remanent magnetization near transitions recorded in the medium. This method of measuring the surface magnetic field can be used to investigate fundamental micromagnetics of media by reading the demagnetized transitions.

To elucidate the mechanism responsible for the relaxation or decay of the perpendicular remanent magnetization of Co–Cr films, Lottis and Dahlberg [9] examined the magnetic after-effect by measuring magnetization continuously using a SQUID magnetometer for time periods of up to 103 minutes. The decays are quasi-logarithmic over at least three decades of time and may be characterized by one of two phenomenological models. A fit to one model's decay rate indicates that the temperature dependence of the decay rate is non-monotonic because the decay rate reaches a maximum in an intermediate region. The latter results are related to thermal excitation and temperature dependence of the demagnetizing field associated with perpendicular magnetization.

1.1.1. Saturation magnetization and related properties

Iwasaki and Ouchi ([34] in Part I) were the first to determine saturation–magnetization values of Co–Cr films. Their results are shown in Fig. 1. The change in M_s with the concentration of Cr agrees with that of bulk alloys, for which M_s decreases almost linearly with the Cr%. The M_s values for selected Co–Cr alloys and pure Co are listed below:

Composition of Film	M_s (e.m.u. cm^{-3})
Pure Co	1,410
Co-10 at % Cr	870
Co-14 at % Cr	620
Co-17 at % Cr	325,390
Co-20 at % Cr	190
Co-25.5 at % Cr	0

At least three groups of workers later reported significantly higher M_s values for Co–Cr films than for bulk alloys of the same compositions. Kobayashi and Ishida [10] first reported that Co–Cr films were ferromagnetic up to 30 at % Cr, in comparison to the 25.5 at % shown in the table above. Then Coughlin *et al.* ([56] in Part I) attained M_s = 500 e.m.u. cm^{-3} in

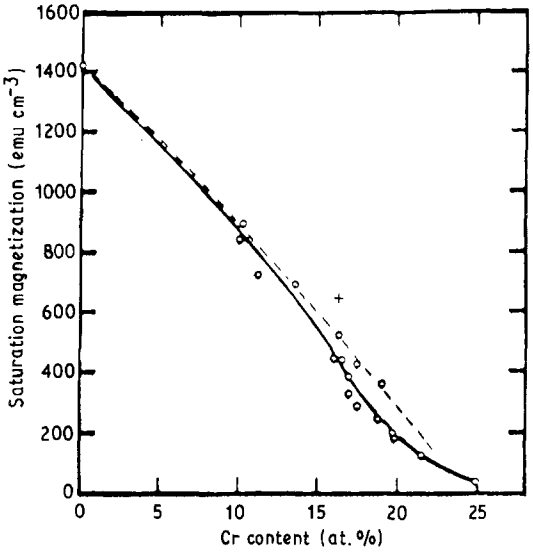

Figure 1 Dependence of M_s on Cr content for Co–Cr films ([34] in Part I.).

the Co-17 at % Cr films, which is 22% (versus 390 e.m.u. cm^{-3}) or 35% (versus 325 e.m.u. cm^{-3}) higher than the values listed in the table. Finally, Wielinga and Lodder (I: [57]) obtained a still higher M_s value of 650 e.m.u. cm^{-3} in the Co-17 at % Cr film, which is either 40% or 50% higher than the listed values.

Haines [11] performed a semi-empirical analysis on the effect of the distribution of constituent atoms on the M_s of Co–Cr films. Assuming that film composition is homogeneous, he calculated M_s by summing up the contribution of Co atoms as a function of the number of Cr atoms in the nearest neighbours. Two models of atomic distribution were adopted: (1) a random array in the hexagonal close packed lattice; and (2) an array with only Co–Co and Co–Cr nearest-neighbour pairs (no Cr–Cr nearest-neighbour pairs). These two models predict the range of M_s values for Co–Cr films produced by radio frequency-diode sputtering, with or without bias voltage applied to the substrate. For cold substrates without bias, the M_s value is expected to be close to that for the random distribution; however, for increasing bias voltage, M_s approaches the value predicted by the model assuming no Cr–Cr nearest-neighbour pairs. For 20 at % Cr, the two models predict $M_s = 480$ and 220 e.m.u. cm^{-3}, respectively. The calculated M_s values are in fair agreement with some experimental data for films containing 11–20 at % Cr. Haines's analysis also explains why sputtered films tend to have higher M_s values than do bulk samples in terms of the two models of atomic distribution.

The discrepancy in M_s between thin films and bulk alloys may also be caused by the deviation of the chromium concentration from the nominal value. Note that the M_s value decreases from 1410 e.m.u. cm^{-3} in pure Co to zero (nonferromagnetic) at approximately 26 at % Cr. Hence, M_s decreases at the (presumably) linear rate of 54.2 e.m.u. cm^{-3} per 1 at % Cr. A deviation of 1–2% of the Cr concentration between the target and film is common in the sputter-deposition process.

Although M_s is an intrinsic structure-insensitive property [7f], varying M_s values have been reported for Co–Cr films of the same nominal composition. Three reasons may be cited for the variation of M_s. First it is difficult, if not impossible, to control the composition and homogeneity of films prepared by the physical vapour deposition (PVD) process. We should therefore not expect the films prepared by three groups of workers (Part I: Iwasaki and Ouchi [34], Coughlin *et al.* [56], and Wielinga and Lodder [57]) to have the same concentration of Cr and the same degree of homogeneity, even though their nominal compositions are fixed at 17 at % Cr.

The second reason involves the annealing of films. In Part I, in Section 4.1.1. on r.f.-diode sputtering, Section 4.1.2. on d.c.-magnetron sputtering, Section 4.1.4. on special sputtering techniques for high-rate deposition, and Section 4.2. on PVD by evaporation, all deposition practices require heating the substrates to temperatures in the 125–250 °C range. These temperatures, although only moderate, are sufficiently high for atomic diffusion, which could affect the homogeneity of the film. For films originally inhomogeneous, the substrate heating could lead to homogenization; however, if the composition of the film is originally homogeneous, the heating could cause segregation of Cr by virtue of atomic diffusion. Both effects are demonstrated by Fujii *et al.* [12], who annealed two types of films: normal Co–Cr films and compositionally-modulated films (i.e. multilayered films with alternating layers of pure Co and pure Cr). Heating the substrates to 450 °C caused interdiffusion of Co and Cr atoms in the films, leading to a reduction of M_s. Heating both types of films at 500 °C, however, increased M_s, $H_{c,\perp}$, and K_u. The increases were explained in terms of the formation of a non-magnetic phase in preferential sites along columnar grain boundaries. Uchiyama *et al.* [13] conducted a similar study on Co–20 at % Cr films prepared by d.c.-magnetron sputtering and found that annealing caused a decrease in M_s. They attributed the decrease to Cr segregation. Further evidence for segregation-induced change in M_s is the observation by Maeda (I: [59]; II: [14]) that the M_s value of Co–Cr films of a fixed composition is strongly dependent on the substrate temperature. In still another study, Snyder *et al.* [15] performed thermomagnetic analyses (TMA) on r.f.-sputtered Co-22 at % Cr films. In the as-deposited state, the films exhibit M_s values higher than the bulk values. On heating, magnetization steadily diminishes to zero at around 700 °C. After cooling from 800 °C, magnetization does not reappear until the temperature falls to < 300 °C. On all subsequent heatings and coolings, the films retain a Curie temperature of ~ 300 °C, but room-temperature M_s values decrease considerably. Such TMA data cannot be explained in terms of Cr-rich oxide formation [16]. Nor can they be explained by Cr segregation in a planar transition layer. The likely mechanisms are Cr segregation at the grain boundaries and atomic-scale redistribution of the chromium.

The third reason that the M_s values of Co–Cr films show strong compositional dependence is unveiled in the study of Thompson and Stevenson (I: [73]). To investigate the influence of oxygen, they mixed argon gas with 0.1–1% oxygen at a partial pressure of 0.01 to 0.1 m Torr for the r.f.-sputtering process. The amount of oxygen incorporated in 1 μm-thick Co and Co–Cr alloy films ranged from 1019 to 1021 atoms cm^{-3}. Although the M_s of the oxygen-doped Co films showed a steady decrease with oxygen content, the M_s of the doped Co–Cr films underwent a steep increase to a peak value at an oxygen concentration of $\sim 8 \times 10^{20}$ atoms cm^{-3}, followed by a sharp decrease at higher oxygen content. The increase in M_s is attributed to Cr's stronger affinity for oxygen, which gives rise to preferential oxidation of Cr rather than of Co. The removal of oxygen and chromium from the solid solution to form chromium oxide is expected to increase the M_s value simply because the final concentration of Cr in the film should be lower than its nominal composition.

Nakamura and Iwasaki [17] performed a statistical computer calculation of the vectorial magnetization to

simulate the magnetic recording process. By applying the incoherent curling mode to magnetization reversal, the calculation restored the measured vectorial M–H hysteresis loop of the Co–Cr film with a coercive force that was lower than the anisotropy field strength. This approach is shown to provide quantitative information on the hysteresis loop for various field directions under PMR conditions.

The magnetization time decay in PMA films of Co–Cr was measured as a function of magnetic field and temperature by Oseroff *et al.* [18] and Webb *et al.* [19]. In place of conventional VSM, the anomalous Hall coefficient was used to determine the magnetization [9]. This method allowed the decay measurements to be made 2 milliseconds after the external field used to saturate the sample was turned off. The decay behaviour was complex but had these salient features: (1) unlike particulate media, in which magnetization decay rate is sharply peaked around the coercive field, the magnetization time decay in Co–Cr films was nearly independent of the external field over a range of several kG; (2) there was a significant deviation from a pure log(t) dependence when examined over 7 decades at 300 K and 4.5 decades at cryogenic temperatures; (3) for temperatures of 10–200 K, decay rates decreased linearly with decreasing temperature; below 10 K, decay rates decreased more rapidly and appeared to approach zero when extrapolated to zero temperature.

The effect of substrate bias (V_s) on the M_s of sputtered Co–Cr films was assessed by Ohkoshi and Kusuda (I:[71]). For sputter-deposited 500 nm-thick films of the Co-23 at % Cr alloy, M_s increased gradually with increasing V_s and reached a constant value approaching that for the bulk alloy when V_s exceeded -125 V. In the absence of compositional change, the bias-induced decrease in M_s was ascribed to the elimination of compositional inhomogeneity in the growing film by virtue of re-sputtering.

Concurrently, Suzuki *et al.* (I:[72]) studied the influence on M_s and M_r (remanence)/M_s of the substrate bias voltage and the accelerating voltage (V_{acc}) of the ion beam used in preparing Co–Cr films. Increasing V_{acc} tends to raise M_s linearly up to $V_s = 1700$ V, but it affects the M_r/M_s ratio very little. The reason for the M_s increase is not clearly known. This study was unusual in that it placed more emphasis on the positive bias, which was extended to 1700 V, than on the negative bias. In any event, negative bias to -500 V seems to have no effect on either M_s or M_r/M_s.

The demagnetization of Co–Cr films was investigated as a function of stress or temperature by Hoshi *et al.* [20]. The loss of remanent magnetization (ΔM_r) was determined as a measure of demagnetization by VSM measurements. The ΔM_r decreased monotonically by roughly 50% as the compressive stress applied normal to the film plane was increased to 4 $\times 10^9$ dynes cm^{-2}. The stress-induced ΔM_r, however, diminished when either the perpendicular anisotropy field ($H_{k,\perp}$) or the film thickness increased. The ΔM_r was also reduced by adopting double-layer media with a soft magnetic underlayer. The latter result implies that the demagnetizing effect is reduced by higher $H_{k,\perp}$ and sharper c-axis texture. Heating the film in its remanent state also led to a decrease in remanence, which was reduced below 85% by heating to 150 °C.

1.1.2. Perpendicular magnetic anisotropy (PMA)

In Part I Section 2.1, we noted that the first requirement of the Co–Cr films for high-density magnetic recording is the formation of PMA. Although thin films of the Co alloys containing more than 13 at % Cr display PMA inherently, PMA is a structure-sensitive property; therefore we have to develop the proper grain structure in order to attain strong PMA. This in turn means that the operational conditions for sputter- or evaporation-deposition must be critically optimized. Indeed, many workers have undertaken studies to correlate the PMA characteristics of the Co–Cr films and the optimal conditions of the fabrication process.

The experimental approach to PMA characterization traditionally involves the following techniques: (a) VSM measurements for the M–H loops, from which the loop shape signifies the preferred direction of magnetization [21]; in one study, Hall-effect measurements were used to secure the loops [22]. (b) torque measurements, from which anisotropy constants K_1, K_2, $K_\perp$, and K_u are calculated (I:[119]); a good example of the torque curve showing nearly perfect PMA in a Co–Cr film is reproduced in Fig. 2 (I:[34]) the curve follows approximately a sin(2θ) relationship. (c) X-ray diffraction (XRD) patterns and the rocking curve of the (00·2) plane, in which the half-width dispersion angle $\Delta\theta_{50}$ is measured. As discussed in Section 5.1, Artman *et al.* [2, 3, 23] applied the FMR technique to investigate the fine structure of PMA films with great success.

Iwasaki and Ouchi (I:[34]) again were the first to apply all three traditional techniques to characterize the PMA of Co–Cr films. They measured the M–H loops of r.f.-sputtered films in two directions: perpendicular ($\perp$) and parallel (//) to the film plane. Fig. 3 shows the // and uncompensated $\perp$ loops for films of three Co–Cr alloys. When compensated for demagnetization, the $\perp$ loops would display a rectangular

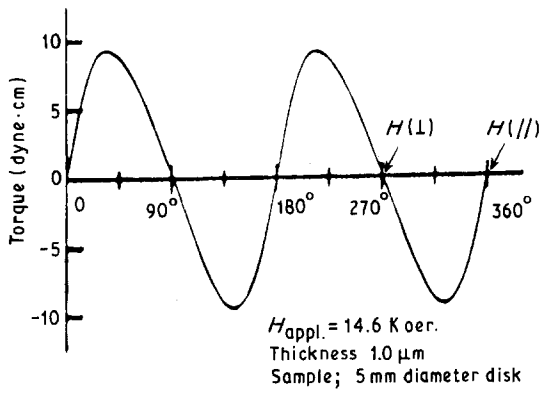

Figure 2 A typical torque curve of the Co–Cr film with PMA (I:[34]).

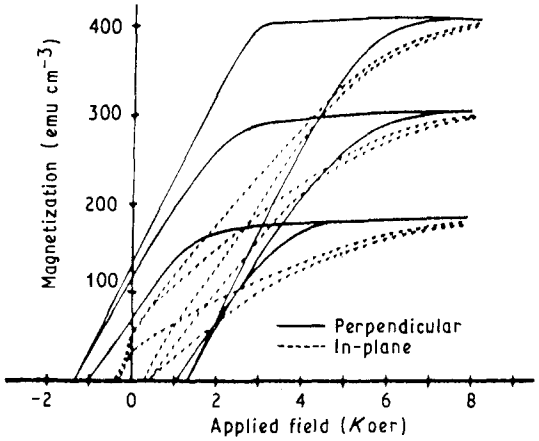

Figure 3 M–H loops of Co–Cr films (I:[34]).

shape with an almost infinite slope. The // loops, however, are isotropic with small hysteresis loss. These results signify that the Co–Cr films have an easy axis of magnetization normal to the film plane and a hard axis in the film plane.

Iwasaki and Ouchi also confirmed PMA by the torque curve measured inside the normal plane of a disk film with $M_s = 300$ e.m.u. cm^{-3} (Fig. 2). The curve is a slightly distorted sine wave with a period of 180°. The polarity and period of the curve indicate that the film has the uniaxial anisotropy whose easy axis lies along the film normal. The uniaxial anisotropy constant K_u was evaluated from the curve using an extrapolation method [24]. The deduced K_u values are listed in Table I and plotted as a function of M_s in Fig. 4 for two deposition rates. As M_s decreases with increased Cr content, K_u rises rapidly from negative values to zero around $M_s = 700$ e.m.u. cm^{-3}, then reaches a maximum of 4.9×10^5 erg cm^{-3} for $M_s = 300$ e.m.u. cm^{-3}. The positive K_u value means that $K_\perp$ surpasses $2\pi M_s^2$, thus allowing the film to be magnetized in the film normal. Equation 3B (Part I) allows the perpendicular anisotropy constant $K_\perp$ to be calculated from K_u and $2\pi M_s^2$. The $K_\perp$ values thus calculated are listed in Column 5, Table I. Although pure Co has the largest positive $K_\perp$ value, the shape anisotropy energy $2\pi M_s^2$ is even larger, keeping K_u in the negative range and disallowing PMA to be formed. Not until the Cr content exceeds ~ 13 at % will the Co alloys show positive K_u for the emergence of PMA. Fig. 4 also suggests that decreasing the deposition rate tends to enhance the perpendicular anisotropy.

Later, Fisher *et al.* (I:[119]) also performed all three types of the traditional measurements on sputtered films of Co-(12.8–23.5) at % Cr alloys. The measurements were aimed at a systematic study of the compositional dependence of M_s, K_1, K_2, $K_\perp$, and K_u, where $K_\perp = K_1 + K_2$. Their results are in qualitative agreement with Iwasaki and Ouchi (I:[34]) with the major difference that the minimum Cr content for positive K_u (therefore for the formation of PMA) is pushed up from Iwasaki–Ouchi's 13 at % to a value of 20.5 at %. This difference may be ascribed to a pronounced segregation of Cr in the sputtered films in the latter study, thus leading to M_s values significantly

TABLE I Saturation magnetization and anisotropy constants of the cobalt–chromium alloys (I:[34])

Composition (at % Cr)	M_s (e.m.u. cm^{-3})	$2\pi M_s^2$	K_u (erg cm^{-3})	$K_\perp$ (erg cm^{-3})
0 (pure Co)	1410	124.9×10^5	-7.2×10^5	117.7×10^5
8.6	950	56.7×10^5	-1.6×10^5	55.1×10^5
10	850	45.4×10^5	–	–
13	700	30.8×10^5	0	30.8×10^5
15.5	500	15.7×10^5	4.0×10^5	19.7×10^5
17	430	11.6×10^5	–	–
18.2	300	5.7×10^5	4.9×10^5	10.6×10^5
20	200	2.5×10^5	4.5×10^5	7.0×10^5

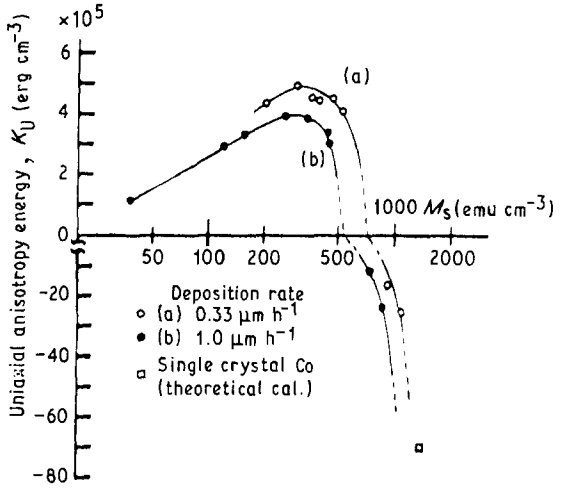

Figure 4 K_u versus M_s in Co–Cr films for two deposition rates (I:[34]).

larger than those reported by Iwasaki and Ouchi and considerably (up to 50%) higher than those measured for the bulk alloys (I:[34]). In a recent study, Ishibashi *et al.* [25] pointed out that the direction of the PMA does not necessarily coincide with the preferred orientation of the c-axis because they may deviate from the film normal at different angles. By introducing two tilt angles (δ for c-axis tilt, η for perpendicular anisotropy axis tilt), the calculation of K_1 and K_2 could be made more accurately from the torque curve. For the PMA films of Co–Cr alloys, the refined analysis should be used when η is greater than 3°. Also, [25] shows that, as the substrate temperature is increased from room temperature to 200 °C, δ is reduced from 6.7° to only 1°.

Iwasaki and Ouchi (I:[34]) were also the first to examine the spread of the preferential alignment of the c-axis in the crystallites by XRD analyses. The $\Delta\theta_{50}$ value of the (00·2) peak was found to vary from 7.5° for the pure Co film to 2.5° for the Co-13 at % Cr film. Their study disclosed not only the origin of PMA being the preferred alignment of the c-axis of the h.c.p. structure in the film normal, but also an effective method for sharpening the c-axis texture (therefore for enhancing the PMA) by lowering the deposition rate. Another factor that influences the sharpness of the c-axis texture is film thickness t_f. Coughlin *et al.* (I:[56]) observed that increasing t_f tends to reduce the $\Delta\theta_{50}$ value. Also seen was the rapid increase of the integrated (00·2)/(10·0) intensity ratio with t_f from less

than 20 for $t_f \sim 0.1$ μm to a maximum plateau value of 370 for $t_f \geqslant 0.8$ μm. Similar dependence of $\Delta\theta_{50}$ on t_f was reported by Wielinga and Lodder (I:[57]), who also observed sensitive deterioration of *c*-axis texture when the argon pressure in r.f.-sputtering at 1.5 kV was increased from 3 mTorr. The effect of P_{Ar} is particularly detrimental above 7.5 mTorr. Another interesting conclusion arrived at by the latter workers and by Hoffman *et al.* (I:[104]) is that the condition $H_{k,\perp} > 4\pi M_s$ expressed in Equation 1B for the onset of PMA is not stringent as far as PMR is concerned. They reasoned that, in thin films, local demagnetizing fields can stabilize a perpendicularly magnetized state in microscopic regions even though the condition expressed in Equation 1B is not satisfied (I:[104]).

Honda and Kusuda [22] obtained hysteresis loops from Hall-effect probing on sputtered films of Co-22.8 at % Cr. In the central region, the loops show perpendicular magnetization characteristics in a wide range of film thickness. However, the *c*-axis begins to tilt from the film normal gradually upon moving away from the film centre, with the tilt reaching as much as 30° at the substrate edge.

For Co–Cr films prepared by the evaporation process, Sugita *et al.* (I:[90]) characterized the PMA by the three conventional techniques. The results are remarkably similar to those observed in sputtered films. The deduced magnetic anisotropy constants and other pertinent data for the evaporated films with or without PMA are summarized below:

	⊥ film	// film
Cr Concentration (at %)	22.6	23.4
Thickness (nm)	150	400
M_s (e.m.u. cm^{-3})	280	260
$\Delta\theta_{50}$ (degrees)	8.2	22.7
$2\pi M_s^2$ (erg cm^{-3})	4.9×10^5	4.2×10^5
K_u (erg cm^{-3})	2.0×10^5	-1.0×10^5
$K_\perp$ (erg cm^{-3})	6.9×10^5	3.2×10^5

Honda and Storer (I:[126]) studied the dependence of PMA properties of evaporated films on the substrate temperature (T_s) and annealing temperature (T_a). The perpendicular anisotropy field $H_{k,\perp}$, $\Delta\theta_{50}$, and $H_{c,\perp}$ show similar dependencies on T_s – they all attain maximum values at an optimal T_s around 250 ± 50 °C. The $\Delta\theta_{50}$ values of 0.3° to 0.4° seem to be unusually low. They also stated that annealing at optimal T_a ($\sim$ 440 °C for maximum $H_{c,\perp}$ and $H_{k,eff}$) can improve the magnetic anisotropy and coercivity of evaporated Co–Cr films.

Chen and Cavallotti (I:[103]) obtained rocking curves for electroplated films of Co–Cr alloys that show an intense (00·2) peak with $\Delta\theta_{50}$ of 9° to 10°. The VSM hysteresis loop measured on the film showing only (00·2) diffraction displays an extremely good rectangular ⊥ loop with an almost infinite slope as in the case of sputtered films described by Iwasaki and Ouchi (I:[34]). Other PMA characteristics of the electroplated films were not reported, however.

Niimura *et al.* [26, 27] conducted two studies with emphasis on the initial formation of PMA in Co–Cr films. One study [26] deals with the effect of sputtering conditions and the interaction between deposit and substrate on the *c*-axis orientation in $Co_{79}Cr_{21}$ films. It was found that facing-targets sputtering (FTS) would be more advantageous than conventional d.c. planar-magnetron sputtering because optimized FTS promotes the *c*-axis orientation by virtue of its plasma bombardment-free substrate condition. This advantage is reflected by the formation of PMA in films deposited on poorly oriented Co–Cr films as the underlayers. If well-oriented Co–Cr films were used as underlayers, a continuing growth of crystallites would lead to further improvement of the *c*-axis orientation in the growing films even under unfavourable sputtering conditions. This Co–Cr underlayer effect persists until the film thickness exceeds roughly 200 nm. The effect is explained in terms of a quasi-epitaxial growth phenomenon. In the second study [27], large values of $(M_r/M_s)_{//}$ and in-plane magnetization were measured in the early stage of deposition with $t_f < 20$ nm. By inserting a 5 nm carbon layer between two layers of 20 nm Co–Cr films, the magnetization in this triple-layered film is essentially perpendicular to the film plane, implying a lower magnetostatic energy for multilayered films than for single-layer films.

Bernstein *et al.* [21] attempted to assess the applicability to PMR of sputtered crystalline films of Co–Cr and amorphous films of $Fe_{75}Tb_{13}Gd_{12}$ by comparing their *M–H* loops and torque curves. Large differences in the perpendicular magnetic behaviour were observed, pointing to a much larger (47 versus 0.5–0.76) quality factor $Q(= K_u/2\pi M_s^2)$ for the Fe–Tb–Gd films. It was therefore suggested that high-density mass disk memories could be more easily fabricated with the iron films than with the cobalt films. The reason for the Co–Cr films showing inferior squareness of the *M–H* loops and in-plane anisotropy is likely to be due to the problems of controlling the Cr content (nominally in the range of 15.9–17.1 at %) or to difficulty in attaining compositional homogeneity in the film.

In magnetic recording, high track-recording density is achieved by using discrete media deposited on grooved substrates. The possible effect of the groove structure on PMA characteristics of Co–Cr films was investigated by Tagami *et al.* [29]. Weakening of the PMA is observed when the groove length is 2.1 μm and groove depth exceeds 65 nm. This effect is attributed to local inclination of the *c*-axis in crystallites caused by the grooved substrate surface, leading to in-plane magnetization, particularly in regions of large M_s and large groove depth.

A comprehensive study conducted on magnetic properties of bias-sputtered Co–Cr films by Ohkoshi and Kusuda (I:[71]) led to the following observations. The intensity of the (00·2) peak increases with the substrate bias voltage V_b, and $\Delta\theta_{50}$ reaches a minimum at $V_b = -75$ V. Further increase in V_b beyond -125 V completely wipes out the (00·2) peak, thus leading to the disappearance of PMA. The latter result is ascribed to "violent Ar ion bombardment", which would produce complete mixing of Co and Cr with random orientation in the film.

In addition to conventional techniques for PMA characterization of Co–Cr films, ferromagnetic resonance (FMR) spectrometry was applied by Artman and co-workers. Several interesting conclusions were drawn from their FMR studies. First, the FMR results prompted Mitchell *et al.* [30] to suggest that Co–Cr films are stratified magnetically (and probably physically) into two layers: the upper or bulk layer is structurally ordered with the *c*-axis texture and a positive effective anisotropy field $H_{k,eff}$; the lower or "transitional" layer, between the substrate and the bulk layer, is a highly disordered, fine-grained region showing a negative $H_{k,eff}$. Later, Artman [23] concluded from a detailed analysis of FMR spectra that the magnetocrystalline anisotropy of the transition layer tends to average to zero, leaving the shape anisotropy dominant. In another study, Mitchell *et al.* [31] reported an $H_{k,eff}$ difference between the free-standing film and the as-deposited film. The $H_{k,eff}$ is attributed to stress (σ)-induced anisotropy. From σ and $H_{k,eff}$, the magnetostrictive constant $A\lambda_s$ can be determined, where A is a constant having the assumed value of 3/2. The λ_s value thus calculated is negative for the bulk layer and positive for the transitional layer. The latter workers further suggest that tensile stresses induced in the Co–Cr films during sputter deposition would increase the positive effective anisotropy of the constituent bulk-type film by as much as 50% and would also increase (in a negative sense) the negative effective anisotropy of the transitional film by as much as 20%.

Niimura and Naoe [32] applied the cantilevered substrate technique described by Klokholm [33] to determine the saturation magnetostriction λ_s of facing-targets-sputtered Co–Cr films. In addition to evaluating λ_s, the determination also serves two other purposes: (a) to detect the presence of the non-magnetic face centred cubic γ phase and (b) to establish a close relationship between *c*-axis dispersion $\Delta\theta_{50}$ and λ_s for both the magnetic h.c.p. ε phase and the γ phase. Consequently, films showing large $\Delta\theta_{50}$ values (e.g. 10°) may be partly attributed to the presence of γ as the minor phase, even though the volume fraction of the γ-phase crystallites is too small to be detected by XRD. The systematic study of Niimura and Naoe also revealed significant roles played by Cr content (Fig. 5), by argon gas pressure P_{Ar} (Fig. 6), and by substrate temperature T_s (Fig. 7) in varying the *c*-axis dispersion $\Delta\theta_{50}$. Seen in Fig. 5 is a steady decrease of $\Delta\theta_{50}$ with Cr content until a minimum plateau value of 2.5° is reached at ~ 18 at % Cr. Niimura and Naoe have thus recommended that the Cr content in the sputtered films should be more than 18 at % to get favourable *c*-axis orientation of ε-phase crystallites. A comparison of Fig. 6 with Fig. 5 indicates that the effect of P_{Ar} on $\Delta\theta_{50}$ is even more pronounced than, but opposite to, that of Cr content. The $\Delta\theta_{50}$ increases rapidly for $P_{Ar} > 3$ mTorr. This adverse effect of P_{Ar} is ascribed to the increase in volume fraction of the γ phase as evidenced by the data for $\lambda_{s,\varepsilon}$ and $\lambda_{s,\gamma}$. The variation of $\Delta\theta_{50}$ with T_s in Fig. 7 follows a tilted S-curve. The lowest $\Delta\theta_{50}$ value of 2.5° occurs for T_s slightly below 200 °C.

The PMA is also characterized by its associated perpendicular anisotropy field $H_{k,\perp}$. This field may be calculated from $K_\perp$ and M_s according to Equation 2 (Part I). Using the data given in Table I, the calculated values of $H_{k,\perp}$ for the Co–Cr films containing 13, 15.5, 18.2, and 20 at % Cr are 8.8, 7.9, 7.1, and 7.0 kOe, respectively. Note that lower $H_{k,\perp}$ is expected in films

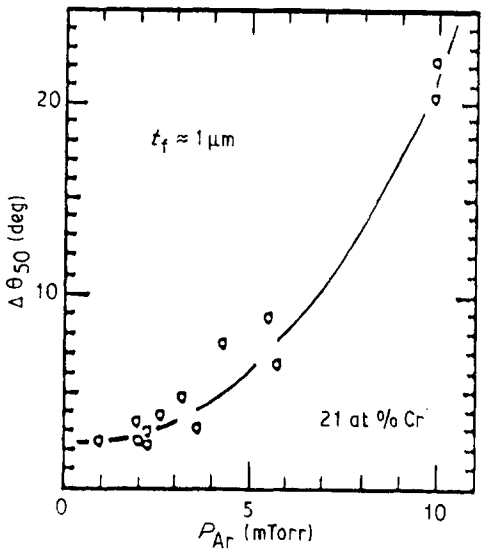

Figure 6 Dependence of $\Delta\theta_{50}$ on argon gas pressure P_{Ar} [32].

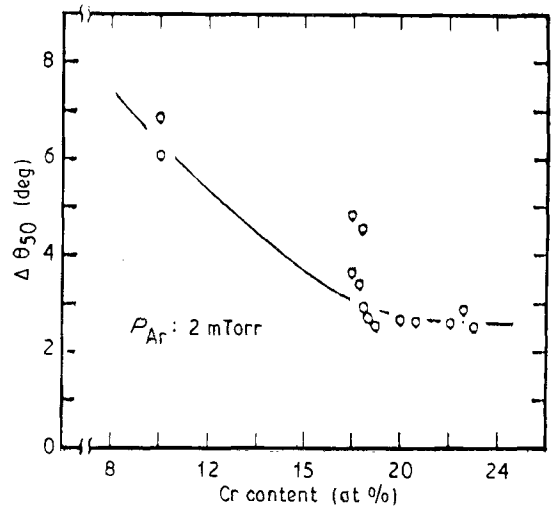

Figure 5 Dependence of *c*-axis dispersion $\Delta\theta_{50}$ on Cr content [32].

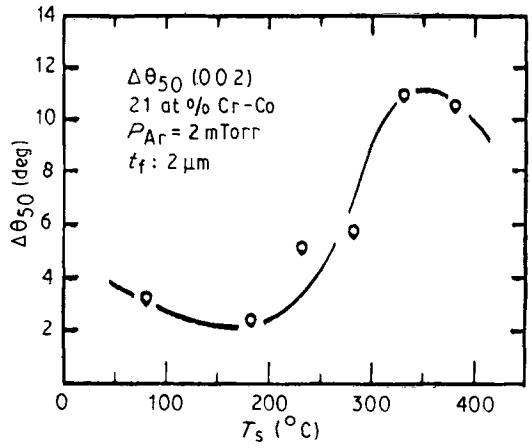

Figure 7 Dependence of $\Delta\theta_{50}$ on substrate temperature T_s [32].

of higher Cr content, therefore of lower M_s (Fig. 1). This dependence is reflected in Equation 2 only if we realize that increasing the Cr content does more than just decrease M_s; it also decreases $K_\perp$ at an even greater rate (data in Table I).

Experimentally, the dependence of $H_{k,\perp}$ on M_s was first reported by Iwasaki *et al.* (I:[44]). Their results are shown in Fig. 8. In the 200–700 e.m.u. cm^{-3} range of M_s values for PMA films, $H_{k,\perp}$ decreases with decreasing M_s (or with increasing Cr content). Such results are consistent with the calculated values of $H_{k,\perp}$. Honda and Storer (I:[126]) presented data for $H_{k,\perp}$ obtained from evaporated Co–Cr films in a plot against M_s. The plot shows a slight increase of $H_{k,\perp}$ with increasing M_s, again in qualitative agreement with the calculation. Wielinga *et al.* [34] found that $H_{k,\perp}$ in r.f.-sputtered, 1 μm-thick films of the Co-16 and Co-19 at % Cr alloys are 7.0 and 3.0 kOe, respectively. Niimura and Naoe [32] studied the dependence of $H_{k,\perp}$ on the substrate temperature and the argon gas pressure (Fig. 9) in facing-targets-sputtered, 1–2 μm-thick films of the Co-21 at % Cr alloy. Fig. 10 shows the variation of $H_{k,\perp}$ with T_s – rising to a maximum value at ~200 °C, then followed by a steady decrease. A similar effect of T_s was later observed in evaporated Co–Cr films by Honda and Storer (I:[126]), who also observed the maximum $H_{k,\perp}$ at 200–250 °C. The effect of annealing temperature T_a on $H_{k,\perp}$, although similar in nature to that of T_s, induces much higher temperatures (> 200 °C more) at which the maximum $H_{k,\perp}$ occurs, however. The dependence of $H_{k,\perp}$ on P_{Ar} is shown in a semi-logarithm plot in Fig. 9 [32]. The decrease of $H_{k,\perp}$ with increasing P_{Ar} is attributed to a corresponding increase in $\Delta\theta_{50}$ (Fig. 6) caused by the increase of volume fraction of the γ phase. Finally, Ludwig *et al.* [35] reported that $H_{k,\perp}$ varies fairly sensitively with the maximum incidence angle (Fig. 11) as a result of change in the target substrate geometry.

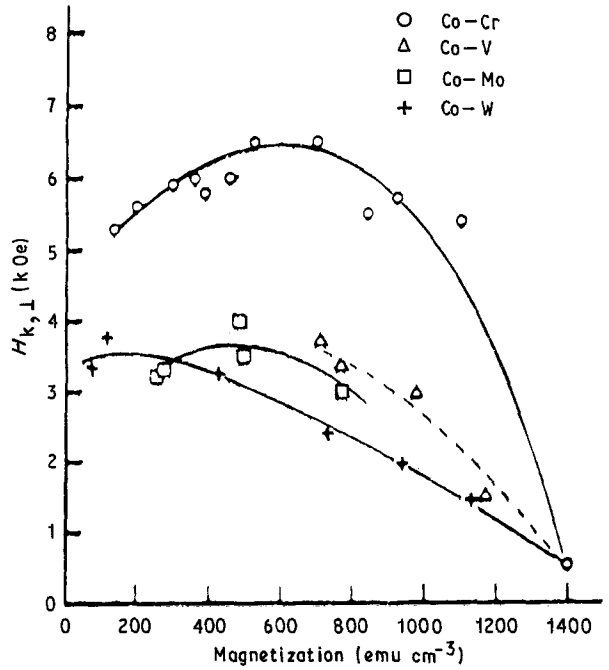

Figure 8 M_s dependence of the perpendicular anisotropy field $H_{k,\perp}$ of Co–M alloy films (I:[44]).

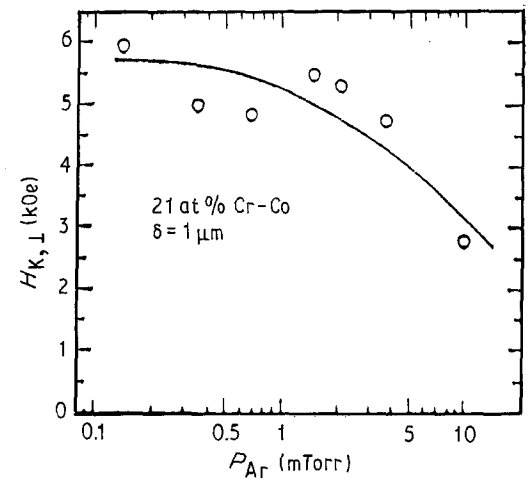

Figure 9 Dependence of $H_{k,\perp}$ on P_{Ar} [32].

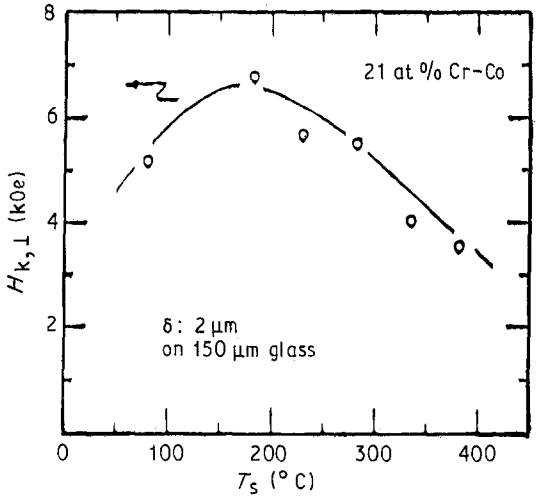

Figure 10 Dependence of $H_{k,\perp}$ on T_s [32].

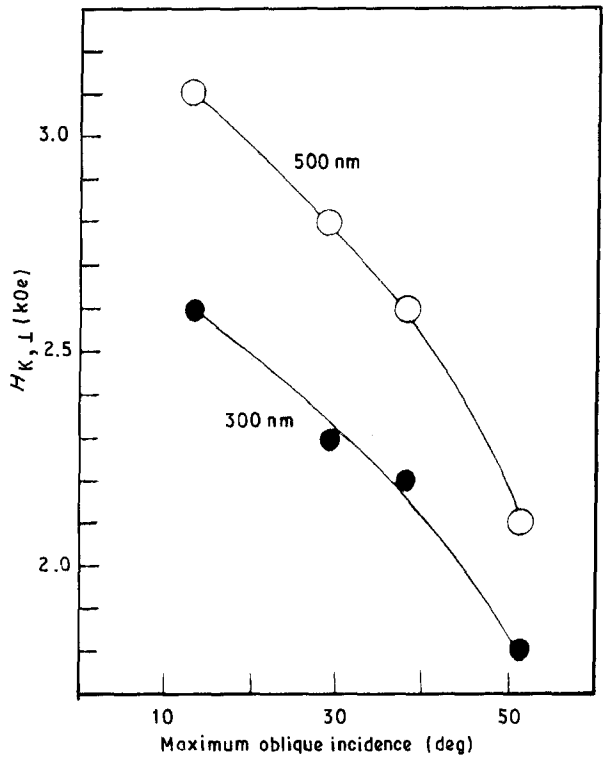

Figure 11 Dependence of $H_{k,\perp}$ on incidence angle for two film thicknesses [35].

1.1.3. Perpendicular coercivity

Although information on coercivity is derived mainly from the M–H hysteresis loop, studies of hysteresis loops will not be reviewed until the next section, when magnetization reversal is discussed. Perpendicular coercivity $H_{c,\perp}$ of the PMA films of Co–Cr alloys is more extensively investigated than any other magnetic properties for three reasons:

1. Coercivity is traditionally considered the most sensitive magnetic property of the grain structure. In view of the versatile conditions under which the PVD process in general, and sputtering in particular, is used to fabricate Co–Cr films, we expect a wide variation in grain structure of the PMA films. Hence $H_{c,\perp}$ is also expected to vary widely according to the conditions of the film-making process. (Later discussion will substantiate this expectation.)

2. In the application of Co–Cr films to PMR, though PMA-related properties ($\Delta\theta_{50}$ and $H_{k,\perp}$) are of prime importance, $H_{c,\perp}$ still plays a significant role, as shown by Wright and Middleton [36]. For efficient application of the PMA film, $H_{c,\perp}$ must be optimized in the desired range (250–1200 Oe). Therefore, $H_{c,\perp}$ must be thoroughly evaluated with respect to the conditions of film fabrication.

3. Coercivity can be determined fairly easily and reliably from the M–H plot. It has been the standard practice of a magnetics laboratory that data from VSM measurements are plotted automatically into an M–H hysteresis loop through simple computer programs.

Experimental results have collectively shown the dependencies of perpendicular coercivity with a variety of fabrication process parameters, notably:

1. substrate temperature, T_s
2. film thickness, t_f
3. deposition rate, dD/dt
4. Cr content or the resulting M_s
5. substrate–target distance, d_{st}
6. sputtering voltage
7. other secondary factors (such as the temperature of post-deposition anneal and the degree of oxygen contamination).

The effect of these parameters will be reviewed separately.

The effect of T_s. The dependence of $H_{c,\perp}$ on T_s was first described by Wielinga and Lodder (I:[57]) and Coughlin *et al.* (I:[56]). Thereafter, it was reported by Maeda (I:[59]), Roll *et al.* [37], Niimura and Naoe [32], Hoffmann *et al.* (I:[104]), Bernards *et al.* [38], and Nakagawa *et al.* [39]. All workers observed the same increasing effect of T_s on $H_{c,\perp}$, which is in contrast to the relative insensitivity of $H_{c,//}$ to T_s between 100 °C and 200 °C. The increase in $H_{c,\perp}$ is rather steep when T_s is raised from 50 °C to 200 °C. Beyond 200 °C, however, the effect of T_s was reported differently between (I:[56, 59]; II:[32]) and (I:[57, 104]; II:[37]).

The results of Maeda (I:[59]), whose study generated the most data points, are shown in Fig. 12. Note

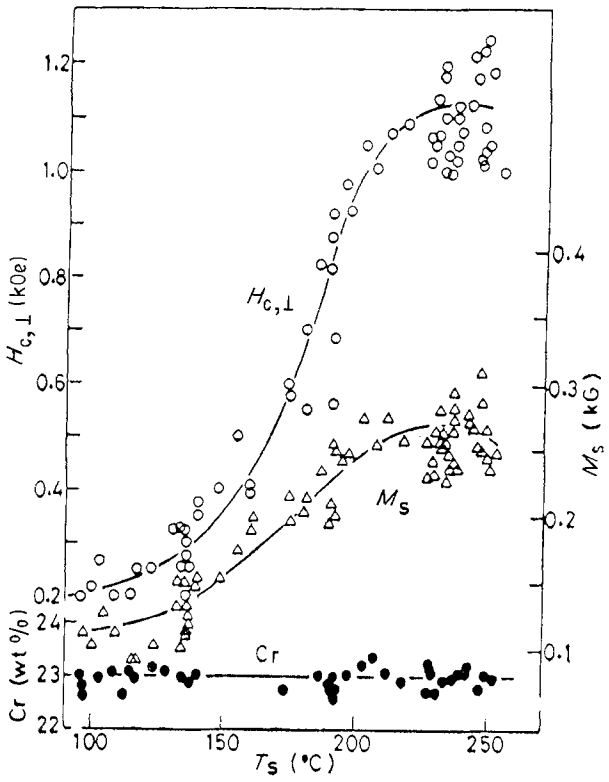

Figure 12 Variation of perpendicular coercivity $H_{c,\perp}$, M_s, and Cr content with T_s for 0.7–2.0 μm thick films prepared at P_{Ar} = 27–36 mTorr. A magnetic field of 60 Oe was applied parallel to the sputtering electric field (I:[59]).

that $H_{c,\perp}$ rises rapidly to a peak value at T_s of about 250 °C. Maeda's conditions for preparing 0.7–2 μm-thick films of the Co–23% Cr alloy were: planar-diode sputtering, fused-quartz substrates, 2.0 kV voltage, P_{Ar} = 27–36 mTorr, and a 60 Oe magnetic field applied parallel to the sputtering field during deposition. Also shown in Fig. 12 are the increase in M_s similar to that of $H_{c,\perp}$ and the constancy of the Cr content in the T_s range of 100 to 250 °C. The increase in M_s is independent of the Cr content, which stays constant. The latter phenomenon is related to the segregation of Cr on the film surface and at grain boundaries, which is promoted by raising T_s.

Further data of Niimura and Naoe [32] show that $H_{c,\perp}$ tends to decrease from the peak value. Correspondingly, there is a decrease in $\Delta\theta_{50}$ from a peak value (Fig. 7) at around 350 °C. Changes in both $H_{c,\perp}$ and $\Delta\theta_{50}$ are attributed to the presence of the non-magnetic γ phase at higher T_s. Results reported in (I:[104]) and [37], however, indicate that the increase in $H_{c,\perp}$ continues up to 400 °C and there is no sign of reversing the trend. Reasons for the discrepancy are not known.

Bernards *et al.* [38] studied the effect of T_s together with that of film thickness on $H_{c,\perp}$. Their results are shown in Fig. 13 for the perpendicular volume coercivity $H_{c,v}$ and surface coercivity $H_{c,s}$ separately in films of varying thicknesses (designated as d in the figure) and T_s (changing in a narrow, 30–90 °C, range). At T_s = 60 and 90 °C, both coercivities show behaviour that is more complex than the slight linear increase at T_s = 30 and 40 °C.

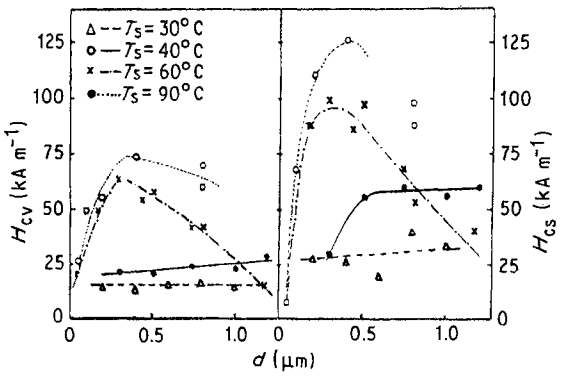

Figure 13 Dependence of perpendicular volume coercivity $H_{c,v}$ and perpendicular surface coercivity $H_{c,s}$ on film thickness for different substrate temperatures [38].

Comparison of perpendicular surface and volume coercivities Smits *et al.* [40] evaluated $H_{c,s}$ and $H_{c,v}$ of r.f.-sputtered films of $Co_{78.5}Cr_{21.5}$. These coercivities were determined by the magneto-optical Kerr effect and by measuring the hysteresis loop with a VSM, respectively. By varying the film thickness from 31 nm to 773 nm, they were able to reveal different changes in the two coercivities together with changes in $\Delta\theta_{50}$ and in the centre-to-centre distance, d_{cc}, between two adjacent columns measured on the surface. Their results are summarized in Table II. For films up to $\sim$ 440 nm thickness, $H_{c,s}$ is larger than $H_{c,v}$, and the difference (1810 Oe versus 1450 Oe) reaches a maximum at t_f = 155 nm. In thicker films, the reverse is true: $H_{c,v}$ decreases to 880 Oe instead of the 380 Oe for $H_{c,s}$. $H_{c,s}$ and $H_{c,v}$ are equal accidentally at $t_f \sim 440$ nm. The differences between $H_{c,s}$ and $H_{c,v}$ are attributed largely to the demagnetization effect at the film surface. Hemmes *et al.* [41] later conducted a similar study. They also detected the reversal in value between $H_{c,s}$ and $H_{c,v}$ at approximately 500 nm film thickness. The physical implication of this reversal in value between $H_{c,s}$ and $H_{c,v}$ was explained in terms of the spike-domain theory, which will be discussed in Section 1.1.1.

The effect of film thickness (t_f) Data for both $H_{c,s}$ and $H_{c,v}$ listed in Table II clearly show an initial increase in coercivity with film thickness until a peak value is reached, then a steady decrease as t_f further increases. This increase-then-decrease trend was detected for $H_{c,\perp}$ by other workers, notably Coughlin *et al.* [56], Nakagawa *et al.* [39], and Ravipati and Haines [42]. The variation of $H_{c,\perp}$ with t_f is a complex phenomenon involving several factors such as the *c*-axis orientation as reflected in the change of $\Delta\theta_{50}$ (see Column 4, Table II), the columnar structure as reflected in the increase of d_{cc} (see Column 5, Table II) and the composition gradient [40] due to progressive depletion of chromium in the Co–Cr alloy target (I:[96]) caused by the different evaporation rates between Co and Cr discussed in Part I, Section 4.2.

Niimura *et al.* [39, 43] investigated the variation of $H_{c,\perp}$ with t_f extensively by (a) altering the geometry of the sputtering target from magnetron to FTS, (b) shifting the structure of films from single to multiple layers, (c) trying different substrate materials (Si, glass, polyimide), and (d) inserting a carbon underlayer. Their results should interest those who want to prepare the PMA films under some of their special conditions of fabrication.

The effect of deposition rate (dD/dt) Coughlin *et al.* (I:[56]) reported that $H_{c,\perp}$ is a function of the deposition rate. Their 1 μm films were prepared with the substrate heated to and held at 170 °C by the r.f.-sputtering process operated at 1.5 kV under 5 mTorr argon pressure. Shown in Fig. 14 are $H_{c,\perp}$, the Cr content, and X-ray integrated intensity from (00·2) plotted against the deposition rate. All three properties display the same variation mode with a peak value appearing at a deposition rate of $\sim$ 0.2 nm/s. These results, coupled with other findings, prompted them to suggest that (a) composition gradients through the film thickness are responsible for the loss of coercivity and (b) the variation of $H_{c,\perp}$ and crystallite orientation seen in Fig. 14 are caused by composition differences induced by changes in relative sputtering rates of the Co and Cr, which are also deposition-rate dependent.

Ouchi and Iwasaki [44], however, later reported that magnetron-sputtered Co–Cr films deposited on substrates held at constant temperatures had perpendicular coercivity dependent on substrate temperature, not on deposition rate. Ravipati *et al.* [42] subsequently found that, when no heat sinking was applied to the substrate during deposition, the temperatures of the substrate and the film would increase with time, leading to a coercivity gradient in the film

TABLE II Variation of $H_{c,s}$ and $H_{c,v}$ with film thickness of the $Co_{78.5}Cr_{21.5}$ alloy [40]

t_f (nm)	$H_{c,v}$ (Oe)	$H_{c,s}$ (Oe)	$\Delta\theta_{50}$ (deg)	d_{cc} (nm)
31	100	900	1.95	50 ± 10
46	990	1570	1.85	105 ± 20
62	1090	1570	1.75	140 ± 25
155	1450	1810	1.40	125 ± 25
309	1400	1600	1.15	180 ± 25
620	900	370	1.10	170 ± 25
773	880	380	1.10	180 ± 30

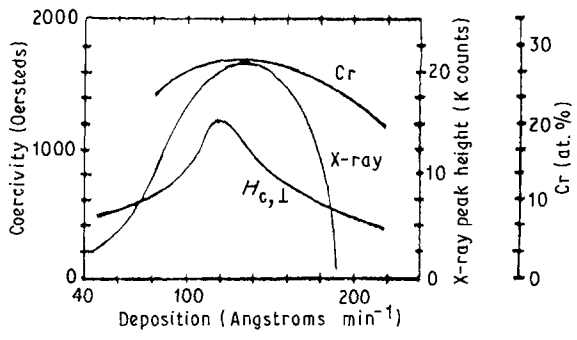

Figure 14 Film properties varying as a function of deposition rate (I:[56]).

that affects both magnetic and recording properties. To ascertain the nature of the coercivity gradient, they performed depth profiling of the films by chemically etching away the material layer by layer, 250 nm in each layer, followed by measurements using the differential vibrating-sample magnetometer (DVSM) technique [1]. Their study unveiled two interesting phenomena. First, $H_{c,\perp}$ exhibits a gradient. For example, the average $H_{c,\perp}$ value of the 250 nm layer removed from the bottom side increases progressively from 66 Oe to 446 Oe. (Detailed results are given in Table III). Second, the initial layers of the film are magnetically soft because their $H_{c,\perp}$ is less than 100 Oe. Therefore, when the film is tested for magnetic recording using a thin-film head, the initial layers act as a magnetic flux sink, as does the Fe–Ni–Cr soft magnetic underlayer in double-layer media. Films with thicker soft layers (using a 10 nm s^{-1} deposition rate) show 30–40% more output in the recording appraisal than did films with thin soft initial layers (using lower deposition rates).

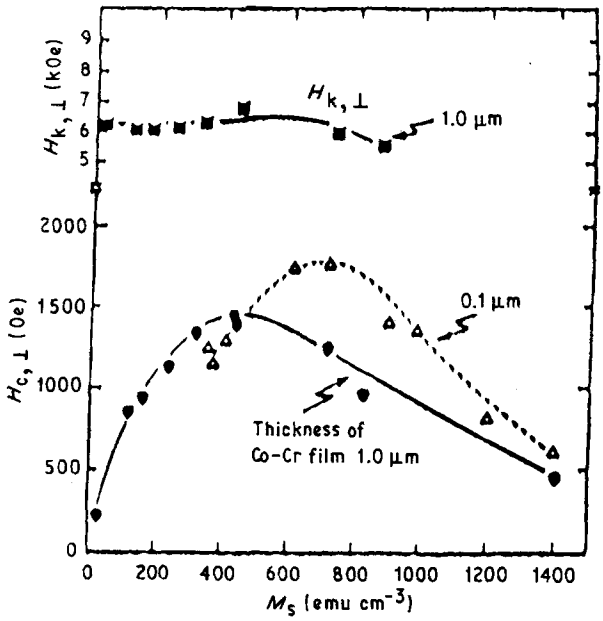

Figure 15 Dependence of $H_{c,\perp}$ and $H_{k,\perp}$ on M_s for Co–Cr films with thickness 0.1 and 1 μm [46].

The effect of the Cr content on M_s Tsumita *et al.* [45] showed the dependence of $H_{c,\perp}$ and $H_{c,//}$ on Cr content. Unfortunately, the results were obtained from composite films with, first Cr, then Co–Cr deposited on a Ni–P/Al disk substrate. Because of the presence of the 0.25 μm Cr underlayer, the films show strong logitudinal anisotropy (evidenced by $H_{c,//} \gg H_{c,\perp}$) when the Cr content exceeds 15 at %. Their results are therefore considered atypical for PMA films in the context of PMA films. Ouchi and Iwasaki [46] later showed the dependence of $H_{c,\perp}$ on M_s (Fig. 15). The plot displays a peak at the M_s value corresponding to the transition from multiple-domain to single-domain behaviour of columns. At lower M_s (or at higher Cr contents), $H_{c,\perp}$ decreases rather rapidly. The peak shifts to a higher M_s value as the thickness of the film is reduced. This dependence demonstrates the flexibility of $H_{c,\perp}$, which enables us to adjust its average value to meet the application specification rather easily. On the other hand, one should be aware that the sensitive $H_{c,\perp}$–M_s relationship may also give rise to local fluctuation of $H_{c,\perp}$ as a result of the Cr segregation so commonly seen in the Co–Cr films.

The effect of substrate-to-target distance (d_{st}) The $H_{c,\perp}$ value was reported to decrease from 1720 Oe (at $d_{st} = 20$ mm) to 1300 Oe ($d_{st} = 74$ mm) in r.f.-sputtered films of Co-(17–19) at % Cr by Wielinga and Lodder (I:[57]). This d_{st} effect is ascribed to the change in induced heating of the substrate. But there may be other factors involved, such as deposition rate, which is known to change with d_{st} according to the relation [47]:

$$\frac{dD}{dt} = \frac{A}{(d_{st})^2}$$

where A is a constant.

The effect of sputtering voltage (V) In the same study (I:[57]), Wielinga and Lodder also studied the dependence of $H_{c,\perp}$ on the voltage of r.f. sputtering; their results are shown in Fig. 16. The $H_{c,\perp}$ increases rapidly with V_{rf} to reach a maximum value at around 1.5 kV for $d_{st} = 34$ mm (around 1.8 kV for $d_{st} = 50$ mm) and stays at the maximum with further increase in V_{rf}. The increase in $H_{c,\perp}$ with increasing V_{rf} is attributed to the enhancement of induced heating of the substrate (i.e. to the accompanying increase in T_s).

The effect of two secondary factors One secondary factor is the temperature of post-deposition anneal,

TABLE III Coercivity profiling of 2 μm films of $Co_{74.8}Cr_{25.2}$ from the bottom side [42]

Thickness (Å)	Average coercivity $H_{c,\perp}$	$H_{c,//}$	DVSM thickness between (Å)	DVSM coercivity $H_{c,\perp}$	$H_{c,//}$
20 000	196	163	–	–	–
20 000–2500	186	169	0–2500	66	49
17 500–2500	239	186	2500–5000	82	66
15 000–2500	289	204	5000–7500	142	108
12 500–2500	323	215	7500–10 000	176	124
10 000–2500	386	243	10 000–12 500	306	203
7500–2500	419	248	12 500–15 000	374	226
5000–2500	431	273	15 000–17 500	411	249
			20 000–17 500	446	264

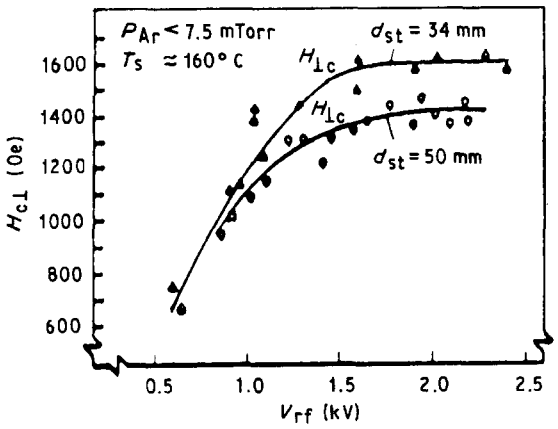

Figure 16 Dependence of $H_{c,\perp}$ on r.f. sputtering voltage V_{rf} for target-to-substrate distances of 34 and 50 mm (I:[57]).

studied by Fujii *et al.* [12]. Besides heat treatment, their study also features composition modulation in films having a multilayered structure with alternating deposits of Co and Cr. Heat treatment up to 450 °C causes interdiffusion of Co and Cr atoms and, at 500 °C, causes increases in $H_{c,\perp}$, M_s, and K_u. These property changes are interpreted in terms of the formation and segregation of a non-magnetic alloy phase.

Another secondary factor is the degree of oxygen contamination. Normally, this factor should not play a role in determining the magnetic properties of the PMA films if the sputtering process is conducted in a relatively oxygen-free atmosphere. Moreover, since Cr has greater affinity for oxygen than Co, selective oxidation takes place with Cr, leaving the Co relatively unaffected. However, two studies were devoted to assessing the oxygen effect. Their results differ significantly. Thompson and Stevenson (I:[73]) reported that $H_{c,\perp}$ is not a function of oxygen content in r.f.-sputtered films but that $H_{c,//}$ begins to rise whenever the oxygen concentration exceeds 1×10^{21} atoms cm^{-3}.

Whatever the effect of oxygen on coercivity, they ascribed it to changes in the coupling between magnetic regions rather than to changes in grain size. Sagoi and Nishikawa [48] detected variations of $H_{c,\perp}$ with the O_2 content between films containing 17 and 25 at % Cr. For these two films deposited without oxygen doping, their $H_{c,\perp}$ values are 1250 and 600 Oe, respectively. For the 17 at % Cr film, $H_{c,\perp}$ is seen to increase slowly with partial pressure of oxygen (P_{O_2}) up to 3×10^{-6} Torr, at which value $H_{c,\perp}$ starts to decrease rapidly together with the deterioration of the *c*-axis orientation. For the 25 at % Cr film, $H_{c,\perp}$ remains constant until P_{O_2} reaches 2×10^{-6} Torr, when $H_{c,\perp}$ begins to decrease. The decrease in $H_{c,\perp}$ is explained in terms of "crystallization degradation" caused by the entrapping of impurity gas atoms.

To conclude this subsection on perpendicular coercivity, it is appropriate to quote the following statement by Lodder *et al.* [49]:

"The coercivity in ferromagnetic layers with perpendicular anisotropy is determined by two factors: 1. The type of magnetization process involved; i.e. is the magnetization reversed by (coherent) rotation or by domain-wall movement? 2. Morphology of the layer; i.e. shape and dimensions of the crystallites (columns), nature of the boundaries, surface and initial layer properties. In fact these two factors are strongly interrelated and their properties are strongly influenced by the deposition parameters such as temperature, P_{Ar}, etc."

1.1.4. Domain structure and the magnetization reversal processes

The PMA films of Co–Cr alloys display different modes of domain structures and special features of magnetization reversal. Information on the domain structure is not only of great interest *per se*, it is also essential for an understanding of how the special process of magnetization reversal comes about. Various observations on the domain structures will be reviewed first.

Starting in 1978, many studies have been conducted on the domain structure of PMA films of Co–Cr alloys by a variety of methods: the Bitter technique (I:[34]; II:[50, 52]), Lorentz transmission electron microscopy [53–57], colloid SEM [58], digitally enhanced Kerr magneto-optical techniques [49, 59, 60], and electron holography [51]. To ease the difficulty in getting a clear understanding of the domain structure of the PMA films, let us first refer to the work by Lee *et al.* [56]. Their study is well co-ordinated and more complete in the sense that they followed the development of the domain structure from the beginning in the growth of the film and they supplemented Lorentz microscopy observations with two structural examinations, TEM on the microstructure, and convergent-beam electron diffraction (CBED) on the crystal structure. Their films were prepared from a target of the Co-22 at % Cr alloy by d.c.-magnetron sputtering, and film thickness varied in the range of 7.5–50 nm so that the films could be examined by TEM and CBED without thinning.

Fig. 17 shows a series of four TEM images of the films with thickness increasing from 7.5 to 15, 40, and 50 nm. Fig. 18 shows the corresponding Lorentz micrographs. The first domain pattern observed in the

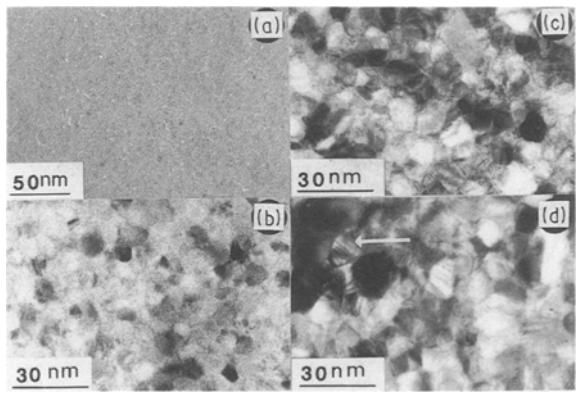

Figure 17 TEM images of Co–Cr films with t_f at (a) 7.5 nm, (b) 15 nm, (c) 40 nm and (d) 50 nm [54].

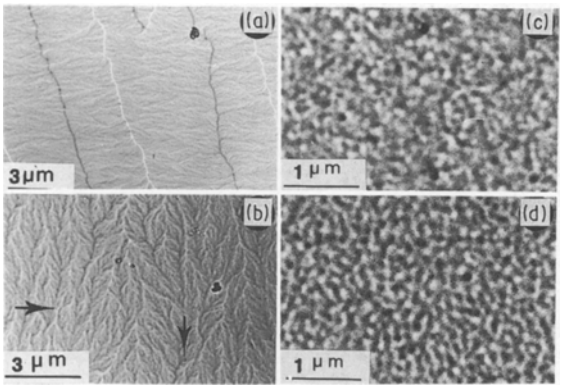

Figure 18 Domain structures seen in the Lorentz images of the same Co–Cr films shown in Fig. 36 [54].

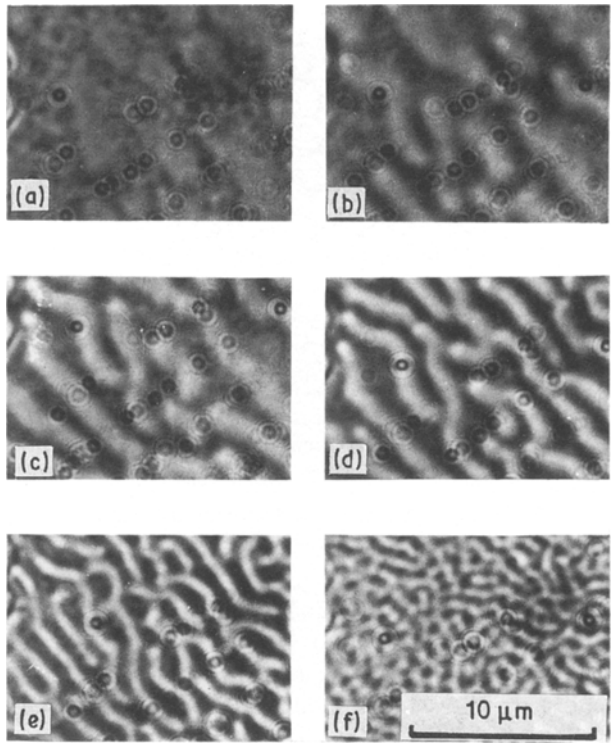

Figure 19 A series of Bitter patterns for a Co–Cr film with $M_s = 545$ e.m.u. cm^{-3}, $K_u = 1.57 \times 10^6$ erg cm^{-3} and $t_f = 1.1$ μm. Stripe domains are clearly seen in (b)–(e) under specified external fields. After the field was further reduced to 1.1 Oe from 3.8 Oe the Bitter pattern shows a maze configuration in (f), which is also observed in the demagnetized state of the Co–Cr films [52].

7.5 nm film (Fig. 18a) consists mainly of in-plane antiparallel domains with these special features: (a) magnetization ripples [61], (b) cross-tie walls [7f], and (c) Block lines of black/white dots along Néel walls [7g]. The TEM image of this extremely thin film (Fig. 17a) and the coupled CBED pattern (not shown) established the presence of an amorphous phase with small crystals in the microstructure. At 15 nm thickness, the domain structure does not show any 180° in-plane domain walls; instead it shows a feather-like configuration together with black and white dots representing small perpendicular components of magnetization (Fig. 18b). The accompanying CBED pattern does not show the diffuse ring; it shows spots occasionally revealing [0 0 0 1] zone axes, but more frequently other zone axes such as [2 $\bar{1}$ $\bar{1}$ 0], [1 $\bar{2}$ 1 $\bar{3}$], and [0 1 $\bar{1}$ 2]. The CBED results together with the TEM image shown in Fig. 17b signify that the microstructure is now crystalline with predominantly randomly oriented grains and a few *c*-axis oriented crystals. In the 40 nm film, the feather-like configuration completely disappears, leaving behind a weak contrast of stripe and dot domains (Fig. 18c). The CBED pattern shows the preferred *c*-axis orientation perpendicular to the film plane in high frequency. Further increase in film thickness to 50 nm results in better contrast of the domain structure of stripes and dots, indicating a further increase in perpendicular magnetization components.

The results of Lee *et al.* typify the varying nature of the domain structure of PMA films of Co–Cr with increasing thickness. The feather-like domain patterns with weak contrast of black and white dots were reported for thin films of Co-(20–23) at % Cr in the early stages of deposition by many other workers, notably Grundy *et al.* ($t_f = 40$ nm) [57], Ohkoshi and Kusuda ($t_f = 20$ nm) [54], and Hoffmann ($t_f = 30$ nm) [55]. The domain structure of stripes was also described for thicker films by many workers: Grundy *et al.* ($t_f = 40$–50 nm) [57], Schmidt and Hubert ($t_f = 622$ nm) [60], Honda *et al.* ($t_f = 1.1$ μm) [52], and Lodder *et al.* ($t_f = 520$–1300 nm for films displaying $H_{c,\perp}$ up to 300 Oe) [49]. The stripe domain configuration has a striking resemblance to that observed on bubble materials (rare-earth orthoferrites, uniaxial garnets, hexagonal ferrites) in the demagnetized or slightly magnetized state [7h]. Fig. 19 shows typical Bitter patterns of stripe domains of an 1.1 μm-thick Co–Cr film with $M_s = 545$ e.m.u. cm^{-3} under an external field of progressively decreasing strength from 5.5 kOe [52].

The domain structure of black and white dots was also recorded from films of similar or greater thicknesses in other studies. Ohkoshi and Kusuda [54] observed in the as-grown film ($t_f = 100$ nm) many dots in the demagnetized state. The underfocused image of the domain structure features blurred white lines partially connecting the dots; overfocusing of the image causes a reversal of the contrast (i.e. white dots are now seen in regions where the contrast is black in the underfocused image). They interpreted the dotted contrast in terms of magnetization curling around the dot. This is the phenomenon in which the in-plane component of magnetization around a column rotates about the central axis of perpendicular magnetization of the column, thus creating a flux closure that acts like a magnetic lens. This gives rise to a dot contrast in the Lorentz micrography imaging [55]. The direction of rotation (clockwise or counterclockwise) plus the condition of imperfect focusing (being either under or over) determines the contrast of the dot as white or black. A schematic illustration of the magnetization phenomenon of curling is given in Fig. 20 [62] together with the analogous spin distribution in a cross-tie wall. Another important finding of Ohkoshi and Kusuda [54] is that the minimum distance between the white and black dots is about 50 nm and roughly corresponds to the spacing between two adjacent

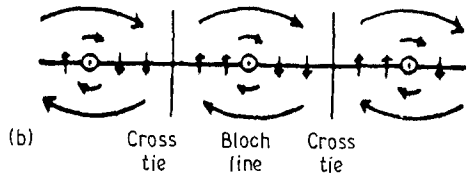

Figure 20 Schematic drawing of magnetization distribution (a) in a 100 nm thick Co–Cr film, and (b) in a cross-tie wall [62].

columns in the film. Grundy *et al.* [57] found that when t_f was increased to 110 nm, the dot contrast became prominent in the Lorentz image of the film and, at $t_f = 210$ nm, the image shows a "completely dot-like contrast". Hoffmann [55] also noticed that "at further increase of the film thickness to 110 nm, the ripple structure has disappeared, leaving only the dot-like structure due to perpendicular magnetization".

In addition to the four types of domain structures (180° in-plane domains, feather-like configurations, stripes, and dots) shown in Fig. 18, the maze pattern has been recorded in the remanent state by Hoffmann [55] and in a nearly demagnetized state by Honda *et al.* [52]. A typical maze pattern, shown in Fig. 19 [52], was originally observed in bubble materials by the magneto-optical Faraday technique [63]. Although PMA films display stripes, dots, and maze patterns similar to the bubble materials, the resemblance between these two types of magnetic materials does not go much further. Actually, they differ vastly in composition and magnetic hardness. Moreover, dot domains in the bubble materials can move swiftly in the lattice under the influence of a bias field [7h], whereas the dots seen on Co–Cr films are created merely through the curling effect around columnar grains under the imaging condition and are immobile because of the stationary columns.

The variation of the domain structure described in Fig. 18 by Lee *et al.* [56] was ascribed primarily to the increase in film thickness in the early stage of deposition. However, the real independent variables that cause the changes in domains are microstructure and degree of *c*-axis orientation. These two variables are explicitly cited by Ali and Grundy [64] and Grundy *et al.* [57], who specify grain size and morphology as the more important features of the microstructure in the analysis here. Other variables affecting the form of domain structures of PMA films are H_c/H_k ratio, magnetic history of the sample, bending created by the deposition process [49], substrate temperature [55], and deposition rate [65].

In view of the many factors suggested, the variation of the domain structure in the PMA films is an extremely complex phenomenon.

When the PMA films are magnetized by a suitable head for high-density recording, the Bitter pattern [58] or the Lorentz image [53] of the energized medium exhibits a simple lamella structure corresponding to elongated stripes spaced with straight boundaries (domain walls). Fig. 21 shows such recorded Bitter patterns on the top and bottom surfaces of a PMR medium containing evaporated 0.15–0.25 μm-thick Co–Cr films (with $M_s = 300$ e.m.u. cm^{-3}) deposited on a 30 nm thick Ge underlayer at 5 kbpi recording density under different write currents [66]. It was pointed out by Iwasaki and Ouchi (I: [34]) that direct observation of the domain structure on the film under high-density recording conditions is very difficult. To circumvent the difficulty, a d.c. field H_a is applied after the film is energized for recording. Goto *et al.* [58] found that the conventional Bitter technique using an optical microscope was efficient in providing clear recorded patterns at 5 and 10 kbpi. At much higher recording densities (such as 50 and 100 kbpi), however, the colloid-SEM method is recommended for better resolution by virtue of higher resolving and magnifying powers of SEM over optical microscopy.

In the interpretation of recorded patterns such as those shown in Fig. 21, Iwasaki and Ouchi (I: [34]) cautioned that, because of the special procedure (energizing for recording, followed by the application of H_a), the stripe spacing is twice as large as the interval of bits. Also, Goto *et al.* [66] have shown that deposits of magnetite colloids on domain walls appear as dark lines in optical micrography, but as white lines in SEM. The distribution of magnetite colloids varies according to whether or not H_a is zero, as schematically illustrated in Fig. 22. For zero H_a, Fe_3O_4 particles deposit on stripe walls (Fig. 6a in [58] and Fig. 22a). For non-zero H_a, e.g. a downward H_a (in Fig. 6b in [58] and Fig. 22b), polarized Fe_3O_4 particles are preferentially attracted to recorded areas or to alternate magnetic domains having the same downward magnetization direction as H_a, instead of depositing on domain walls. A reversal of H_a means shifting the polarized Fe_3O_4 particles to the other set of recorded areas or the neighbouring domains, so the image itself will be reversed. Note the image reversal between

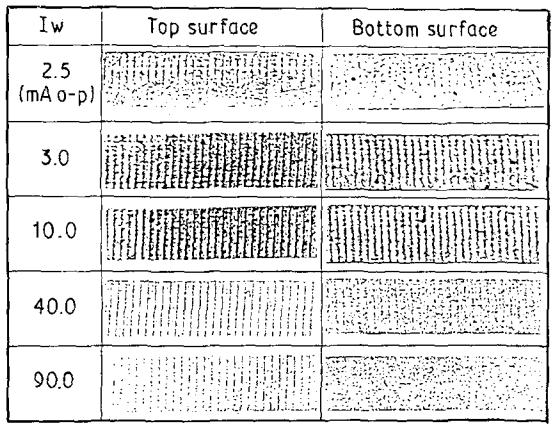

Figure 21 Bitter patterns of 5 kFCI recording seen at the top and bottom surfaces with different write currents [66].

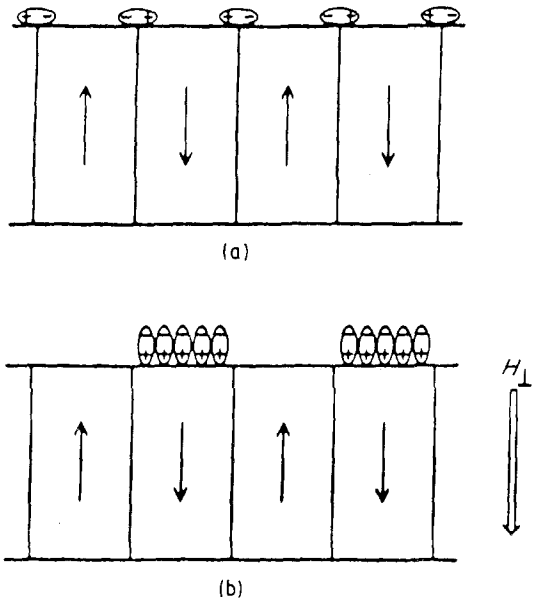

Figure 22 Distribution of magnetite particles on the surface of a Co–Cr film with (a) no field and (b) a field applied downward [58].

Fig. 6b and c in [58] as a result of the reversal of the direction of H_a. Goto *et al.* determined the mean width of the stripe patterns (bit width, w_b) by measuring the width of the band image of stripes. The measured values of w_b are 5.4, 2.3, 0.60, and 0.28 μm for recording densities 5, 10, 50, and 100 kbpi, respectively. These measured bit widths are in reasonable agreements with the calculated values: 0.51 and 0.25 μm for 50 and 100 kbpi, respectively.

The magnetization reversal of PMR media drew attention at the outset of the development of Co–Cr films. To appreciate what might be looked for here, we recall that fast switching in thin film generally relies on coherent rotation of spins across domain walls, not on domain-wall motion [71]. For perpendicular magnetic recording, emphasis is first placed on high bit density, however. Translating this emphasis into grain and domain structures, columns with their *c*-axes preferentially oriented normal to the film plane must be kept as small as physically possible, and each column must be a single domain even in the remanent or demagnetized state. Moreover, many workers believe that thin films with PMA should display not only rectangular hysteresis loops, but also additional features of magnetization reversal to simple rotation. Indeed, the hysteresis loop of a typical PMA film with the magnetizing field applied normal to the film plane was shown in the early work of Iwasaki and Ouchi (I:[34]) to be nearly rectangular, provided the M–H loop is compensated for demagnetization (Fig. 13). A special feature of the hysteresis loop of a PMA film is the deviation from unity slope at $M = 0$. In other words, we expect the slope:

$$T = \left(\frac{dM}{dH}\right)_{M=0} = 1 \qquad (1)$$

Wielinga and Lodder [67] noted from measurements on sputtered Co-19 at % Cr films of 25–625 nm thickness that the slope always deviates from, and is greater than, unity. Moreover, the deviation rises

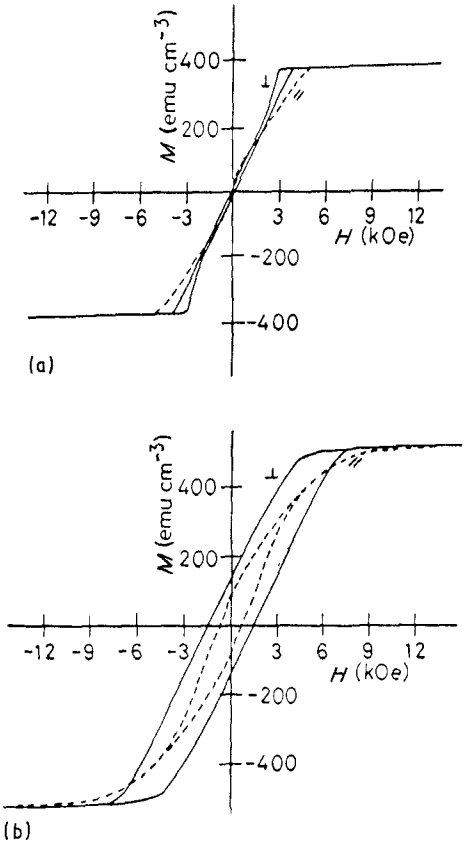

Figure 23 Perpendicular (—) and in-plane (- - - -) hysteresis loops of Co–Cr films sputter-deposited on substrates at (a) 27 °C and (b) 150 °C [69].

rapidly when the film thickness falls below 200 nm. They called this phenomenon shearing of the hysteresis loop. The term shearing is a bit misleading because the loop is not cut and displaced at the coercivity points. Originally, the phenomenon was thought to be difficult to understand based strictly on a particle model. Later, Chang and Fredkin [68] claimed that a simple three-dimensional particulate model coupled with proper selection of separation distances of the columns can explain the phenomenon quite well. Honda and Takahashi [69] observed a sensitive variation of the loop shape with the substrate temperature T_s. Fig. 23 shows that raising T_s from 27 °C to 150 °C would increase coercivity significantly and replace the sharp shoulder by a sloping shoulder.

The hysteresis behaviour of PMA films was further studied by examining the domain structure by the Bitter technique at various strategic points along the loop (especially around the shoulder) by Schmidt and Hubert [60], Honda and Takahashi [69], and Lodder *et al.* [70]. Their observations were similar, particularly on the so-called "nucleation and strip-out" phenomena [60]. Some representative observations reported by Honda and Takahashi [69] are shown in Fig. 24. The r.f.-sputtered Co-23 at % Cr film used to obtain Fig. 24 is 1.1 μm thick and displays $M_s = 340$ e.m.u. cm^{-3}, $H_{c,\perp} = 92$ Oe, $H_{c,//} = 98$ Oe, $K_u = 7.7 \times 10^5$ erg cm^{-3}, and $\Delta\theta_{50} = 3.5°$. From the saturated state, on decreasing of the applied perpendicular field, a few bubble-like reverse domains (white dots–do not confuse with the small round

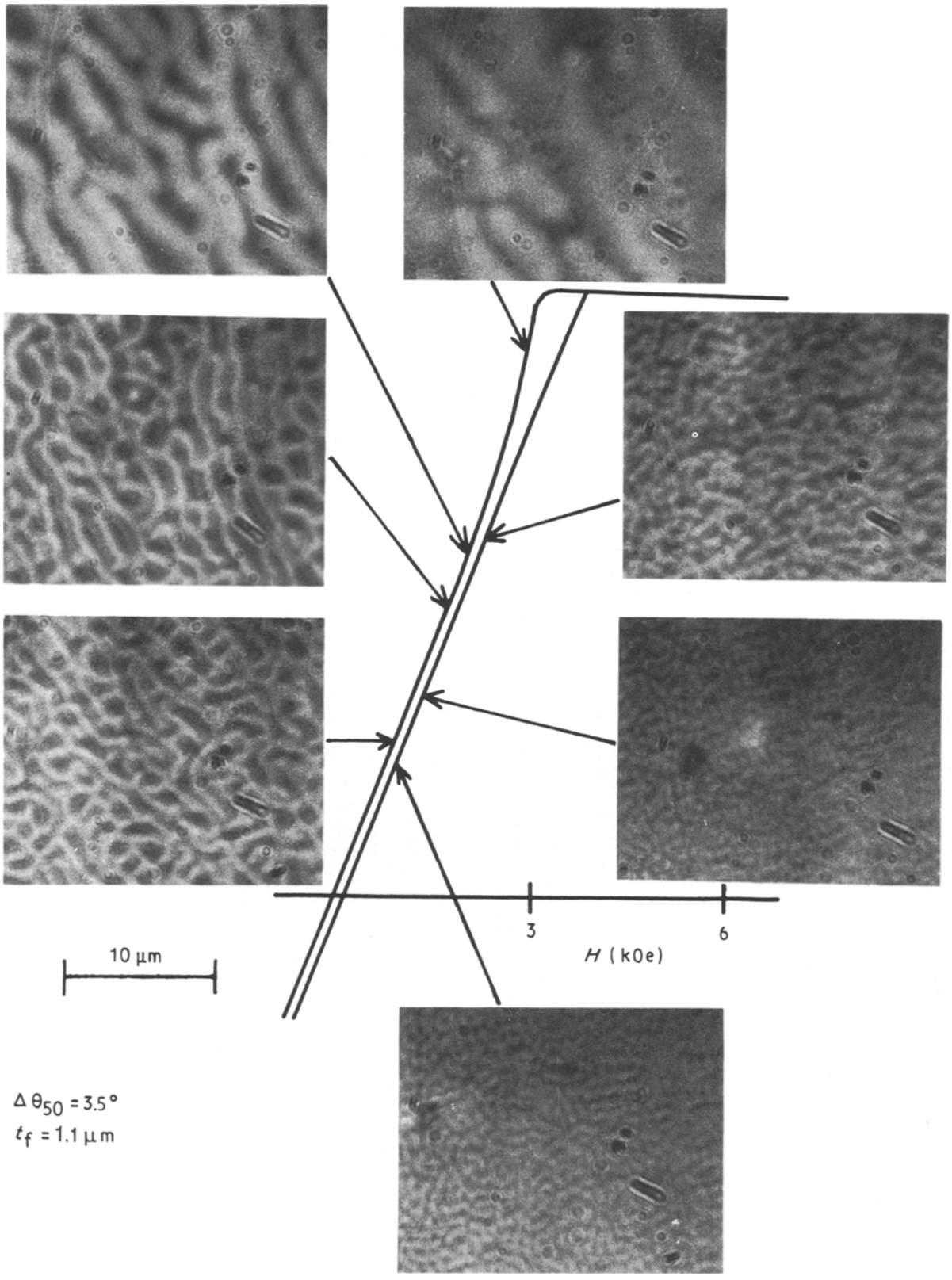

Figure 24 Changes in domain structure seen in a series of Bitter patterns taken along the hysteresis loop. Note the nucleation and growth of reversal domains in three Bitter patterns taken after passing the sharp shoulder [69].

particles representing nodular defects on the film surface that are seen in all micrographs in the figure) nucleate at the loop shoulder. The reversed domains then grow into long stripe domains by domain-wall motion, leading to the eventual maze pattern. This series of observations represent the typical "nucleation and strip-out" phenomena. The elaborate study involving hysteresis-loop tracing and domain-observation notwithstanding, it sheds little light on the mechanism of magnetization reversal. In fact, the work of Honda and Takahashi [69] led to the spurious conclusion that the magnetization reversal process "arises mainly from the wall motion". According to Lodder *et al.* [70], magnetization reversal in the columns needs to be studied by more sophisticated electron microscopy observation methods, such as digitally-enhanced Kerr

microscopy, and with other techniques (e.g. neutron depolarization and surface coercivity measurements).

In other studies, the elucidation of the process of magnetization reversal in PMA films can be categorized into two approaches: (a) Experimental coupled with semi-theoretical analysis and (b) computer simulation. In the first approach, an effective criterion must be adopted for choosing an appropriate magnetic property of the hysteresis loop so that the angular dependence of the property can be calculated with respect to the various reversal mechanisms. By measuring the angular dependence of the chosen property and by comparing the measured data with the calculated results, the criterion should be able to differentiate the validity of different mechanisms.

Early (1980) in this approach, coercivity was used as the criterion (I: [44]). In a 1986 study, Byun *et al.* [71] used coercivity as well as the rotational hysteresis-loss parameter R_h as criteria for ascertaining the mechanism of magnetization reversal. The parameter is defined by:

$$R_h = \int_0^{\theta} \frac{W_r}{M_s} d\left(\frac{1}{H}\right)$$

where $W_r = \int_0^{2\pi} L \, d\theta$, with L being the torque in the sample and θ being the angle between the applied field and the easy axis. The angular variation of coercivity for the initial layer, 80 nm in thickness, of the r.f.-diode-sputtered film indicated reversal by domain-wall motion. For thicker films in the 0.3–1.5 μm range, R_h data signify that coherent or incoherent rotation controls the reversal mechanism. They also found that the reversal mechanisms are independent of the dispersion of orientation of the films. In a 1987 study, Ouchi and Iwasaki [72] came to realize that coercivity is too sensitive to the presence of the initial layer in the PMA films to serve as a reliable criterion. The formation of the initial layer and its influence on the overall recording characteristics of thin films were described by Byun *et al.* [73, 74] and Niimura *et al.* [27]. Further discussion on the initial layer will be given in Section 2.

The new criterion adopted by Ouchi and Iwasaki [72] is hysteresis loss. The angular dependence of the loss, i.e., the variation of loss with the angular position, Ω, of the applied field relative to the easy axis of magnetization in the film normal (see inset of Fig. 25c), is then calculated with respect to three mechanisms of magnetization reversal: rotation of the Stoner–Wohlfarth (S–W) model [75], domain-wall motion, and the curling mode [76]. Figure 25a shows the calculated results for the three mechanisms when hysteresis loss is normalized by the loss at $\Omega = 0°$ and the parameter S for the curling mode is defined by $S = R/R_0$ with R being the column radius and $R_0 = A^{1/2}/M_s$, A being the exchange constant.

To refine the calculation for the curling mode, it is assumed that the easy axis of magnetization may not be completely oriented in the film normal as reflected by a finite value of the volume ratio r of the in-plane orientation part of the c-axis. The calculated curves of the curling mode for $S = 1.2$ and $r = 0$–50% are shown in Fig. 25b. The measured hysteresis losses in the entire 0–90° Ω range are plotted for typical PMA films of four thicknesses in Fig. 25c. A comparison between the measured data and calculated results in Fig. 25 readily reveals that the domain-wall motion model is effective when the film is only 25 nm thick. The reversal behaviour in the thicker 38 nm film supports the S–W model of rotation whereas the curling mode appears to work well for still thicker films with non-trivial amounts of in-plane orientation of the easy axis.

In conclusion, Ouchi and Iwasaki emphasize the versatility of the curling mode capable of explaining

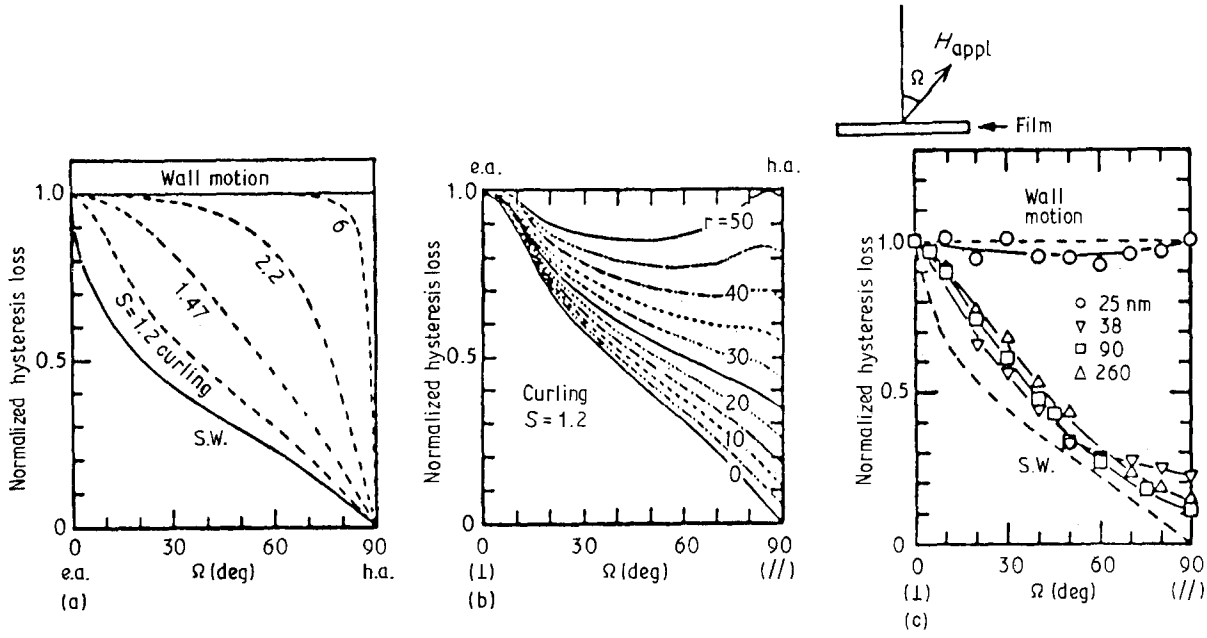

Figure 25 Calculated angular dependence of hysteresis loss for (a) several modes of magnetization reversal, and (b) the curling mode of $S = 1.2$, while the in-plane easy axis is assumed to have various volume ratios r to the total. (c) Observed angular dependence of normalized hysteresis loss for various thicknesses of high $H_{c,\perp}$ Co–Cr films [72].

the reversal behaviour in terms of the hysteresis-loss angular dependence of the majority of PMA films. In a follow-up analysis, Li and Lodder [77] examined the variation of hysteresis loss ($W_h/W_{h,\perp}$) and orientation ratio (OR = $S_\perp/S(\theta)$, where θ is the angle between the applied field H_a and the film normal, $S = M_r/M_s$) as functions of amplitude and direction of the applied field for low (< 2) and high (> 10) $H_{c,\perp}/H_k$ r.f.-magnetron-sputtered Co–Cr films. They concluded that the reversal behaviour depends strongly on the amplitude and direction of the field, and the initial layer has an important influence on the type of reversal. They further concluded that the rotation mechanism governs the switching in high $H_{c,\perp}/H_k$ films whereas the domain-wall reversal acts in the low coercivity films.

In a separate study that involved measuring surface and volume hysteresis, Hemmes *et al.* [41] proposed that magnetization reversal could be effected by the formation and growth of spikes at the surface of films thicker than a critical value $t_{f,c}$. Typically, $t_{f,c}$ is 180 nm for r.f.-sputtered films and 300 nm for d.c.-magnetron-sputtered films of the Co-19 at % Cr alloy. In 1986, Herzer *et al.* [78] described a theory of nucleation fields for homogeneous rotation in uniaxial ferromagnets. Their theory in essence modifies the Stoner–Wohlfarth model by incorporating the second anisotropy constant for a more critical calculation of the nucleation field. Up to this writing, the new model has not been applied in place of the old Stoner–Wohlfarth model to the PMA Co–Cr films.

In the second approach, computer simulation is performed under certain assumed conditions. Zhu and Bertram [79] base their simulation on the model that the film has a columnar structure in which each column is assumed to be a single crystal with perpendicular uniaxial crystalline anisotropy and always uniformly magnetized even during its magnetization reversal. The gyromagnetic equation of motion with phenomenological Landau–Lifshitz damping is then used to describe the magnetization rotation of this coupled system. The computation focuses on the collective magnetization reversal modes of the particles due to magnetostatic interactions and intergranular exchange coupling. It yields coercivities equal to or less than the crystalline anisotropy field, $H_k = 2K/M_s$. They argue that, due to this collective process, the uniform rotation reversal mechanism for the individual particles in the film is energetically more favourable than non-uniform reversal, such as curling. Intercolumn exchange coupling significantly reduces the coercivity, and an increase of the exchange coupling strength changes the magnetization behaviour from "particulate" to "continuous".

1.2. Other PMR-related properties

Certain mechanical and chemical properties of PMA films are important in the application of the films to high-density magnetic recording. Specifically, the resistances to wear and corrosion are of particular concern. If the films are highly susceptible to either mechanical wear or chemical attack, the endurance and reliability of the recording media will be seriously impaired and their useful lives greatly shortened.

1.2.1. Wear resistance

For PMA films to be durable in the PMR application, they must have satisfactory mechanical properties to resist the abrasion of the read/write head. Motomura and Tagami [80] characterized the wear resistance of r.f.-magnetron-sputtered films of Co-(0–33) at % Cr alloys by evaluating the tensile strength and Young's modulus as functions of the sputtering pressure and Cr concentration. Partial results of their work are shown in Figs 26 and 27. For the Co-18 at % Cr films, the tensile strength and Young's modulus decrease rapidly when P_{Ar} exceeds 2 mTorr (Fig. 26a). According to Archard's adhesive wear theory [81], elastic wear volume may be defined as approximately

$$V_{elastic} = Ts/E$$

where T is the tensile strength, s the sliding distance, and E Young's modulus. The calculated values of $V_{elastic}$ from the results in Fig. 26a are shown in Fig. 26b. From the standpoint of adopting wear volume as a measure of the wear resistance, low sputtering pressures are favoured. Specifically, for the Co-18 at % Cr films prepared by r.f.-magnetron sputtering, argon pressures < 4 mTorr are recommended. The dependence of tensile strength and the corresponding elastic wear volume on the concentration of Cr is shown in Fig. 27a and b for P_{Ar} = 1 and

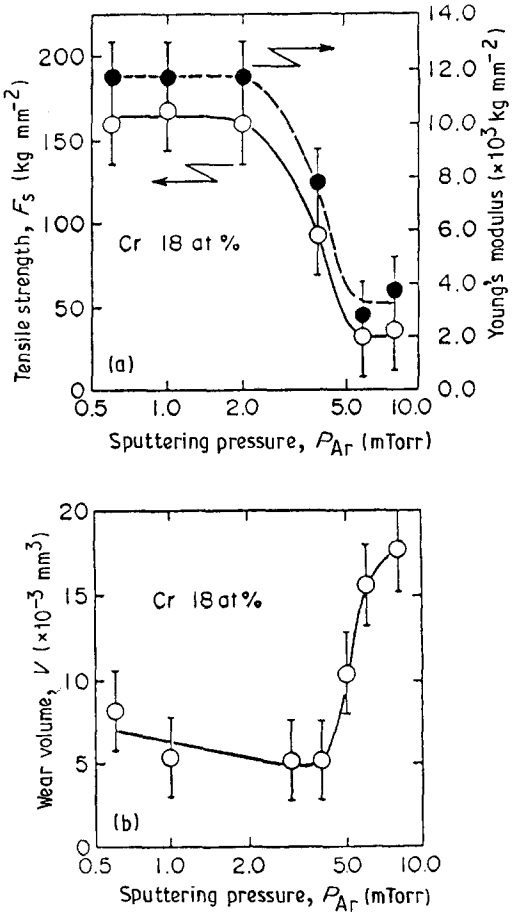

Figure 26 Variation of (a) tensile strength F_s and Young's modulus E, and (b) wear volume V with P_{Ar} for Co-18 at % Cr films [80].

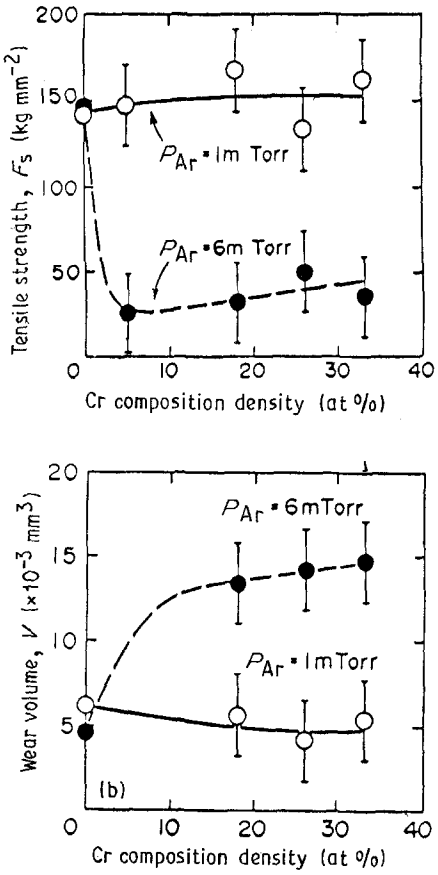

Figure 27 Variation of (a) F_s and E, and (b) V with Cr content of Co–Cr films prepared at $P_{Ar} = 1$ and 6 mTorr [80].

6 mTorr, respectively. Although little variation is seen in T and $V_{elastic}$ up to 33 at % Cr for $P_{Ar} = 1$ mTorr, a large and sudden jump in both properties is seen in the 0–10 at % Cr range with $P_{Ar} = 6$ mTorr. Microstructural analyses on the Co–Cr films indicate that a main factor that affects the tensile strength and wear resistance is the Cr segregation at grain boundaries. The data of Motomura and Tagami provide some guidance for the choice of Cr% and sputtering pressure as far as the wear resistance of the Co–Cr films is concerned.

Three studies were devoted to characterizing the wear behaviour of Co–Cr films in various PMR media under certain operating conditions of a specific recording head. Yamaura *et al.* [82] evaluated tribologically the wear properties of sputtered Co–Cr/permalloy double-layered film on a flexible substrate with or without a 20 nm-thick, inorganic protective coating in contact with dummy heads of different materials. Better wear resistance was observed when (a) the head slider was made of hard materials such as $Al_2O_3 \cdot TiC$ instead of soft materials such as glass, (b) the surfaces of both the PMA film and the head slider were smooth, and (c) the protective coat was present. After 10 million passes of an $Al_2O_3 \cdot TiC$ spherical head, the output signal loss was less than 3 dB. Furuya and Nakayama [83] characterized the extent of wear of Co–Cr thin-film media in relation to the running velocity, radius, and load of the spherical dummy head. Wear was found to depend strongly on the velocity between the head and the medium. Wear resistance was improved by higher head velocities. When the velocity exceeded 1 m s^{-1}, however, the air space between the medium and the head was increased and the friction coefficient decreased. It should be cautioned that even though air lubrication generally subdues wear, increasing air flow may not be desirable in high-density recording because it may cause severe loss of output in the read/write process. Another measure to improve the wear resistance of flexible PMR media is the protection of the film surface from scratches. Kadokura *et al.* [84] evaluated the tribological behaviour of a double-layered recording disk medium consisting of a flexible substrate, a permalloy underlayer, a sputtered Co–Cr film, and an inorganic protective coating. The metallurgical process by which the durability of signal production of the medium deteriorated was elucidated. Brittle fracture or plastic deformation of the disk was found to be responsible for the deterioration. A disk capable of deforming plastically shows better signal durability than that from a disk with brittle fracture. High toughness and homogeneous structure of metal layers improve the signal durability.

Artificial methods are available for the improvement of the wear resistance of PMR media. A conventional method is the use of lubrication fluid [85]. But the foremost measure is to coat the PMA films with a thin layer of carbon, preferably of diamond-like high hardness and other properties. A comprehensive review of the numerous studies on the preparation and properties of diamond-like carbon (DLC) films was undertaken by Tsai and Bogy [86]. Unfortunately, the review made references only to (longitudinal) particulate media in computer hard disks for data storage, with no reference to PMR media. In the final comments on the application of the DLC films as overcoats on thin-film media, they concluded that "At present, when the commercial application of carbon overcoats has gone farther than the scientific understanding of this thin-film material, further development in technology might totally depend on the fruitful results of structure-property research on carbon thin films". This conclusion signifies that very little developmental work is required to apply the technology of DLC overcoating to PMA films.

Kurokawa *et al.* [87] described a new method, known as Plasma Injection CVD (PI-CVD), for depositing DLC films on ferromagnetic metallic films. The main impetus for devising the PI-CVD method is the deposition of DLC films at a rate up to 6 nm s^{-1} at room temperature. This allows recording media to be made in the tape form involving low melting-point polymeric substrate tapes such as PET. The DLC coatings thus prepared show high hardness readings and low friction coefficients, but their structure deviates from diamond and graphite. Both scratch tests and rotary-head still tests demonstrate that the DLC coating indeed improves the durability of the medium. For instance, no degradation in signal output was observed after 10^7 passes whereas tapes without DLC coating showed a breakdown after 2×10^4 passes. Nagao *et al.* [88] applied d.c.-magnetron sputtering at a power density of 3 W cm^{-2} to deposit a carbon coating on composite films of 200 nm Co–Cr and

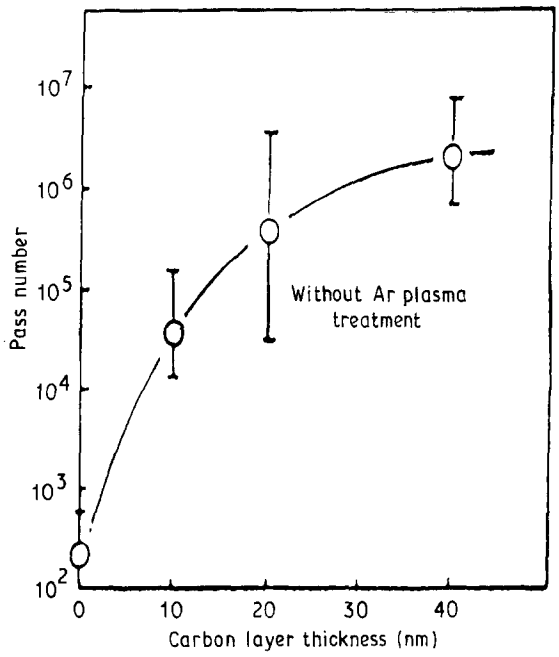

Figure 28 Number of passes versus thickness of the protective carbon film [88].

500 nm Ni–Fe–Mo. Although the structure of the carbon layer was described as graphite-like–not diamond-like–and amorphous, the presence of the carbon coatings improved the durability of the composite film greatly, and the improvement was further enhanced rapidly with the increase in coating thickness up to 40 nm, as shown in Fig. 28.

With regard to the structure, according to a 1985 report by Savvides and Window (reference 30 in the review by Tsai and Bogy [86]) and this reviewer's unpublished work, d.c.-magnetron-sputtered carbon films at low power densities are diamond-like in hardness and other mechanical properties, even though X-ray diffraction shows typical diffuse-ring patterns signifying the amorphous state.

1.2.2. Corrosion resistance

Before focusing our discussion on the corrosion properties of PMA films, we should briefly mention their oxidation behaviour as follows. (The effect of oxygen on the magnetic properties of PMA films was discussed in Part I, Section 3.3.2.) As is well known, chromium is widely used for alloying with other metals because of its protective action against oxidation internally in the matrix of the alloy and more importantly through the formation of a thin, tenacious layer of Cr_2O_3 on the surface. Stainless steels and the renowned nichrome (65% Ni, 20% Fe, 15% Cr) are two noted cases. Also, the work of Ohkoshi *et al.* (I:[47a]), reviewed in Part I, Section 3.3.1, has illustrated this point clearly. Honda *et al.* [89] examined the effect of annealing in air near 400 °C on magnetic properties of Co–Cr films. Considerable increases were recorded in M_s, $H_{c,\perp}$, and $H_{k,\perp}$. These increases were attributed to the formation of antiferromagnetic Cr_2O_3 at the column boundaries as a result of selective oxidation of Cr. Kugiya *et al.* (I:[47b]) described the adverse effect of oxygen contamination of Co-23% Cr evaporated films on PMA properties and recording characteristics in details.

The corrosion behaviour of the Co–Cr films has been characterized in a variety of ways. Sugita *et al.* (I:[90]) were early workers who revealed superior corrosion resistance of evaporated Co–Cr films in tests involving six months exposure to a 90% relative humidity (RH) atmosphere at 60 °C. They detected a protective, thin (< 5 nm) layer of oxide, presumably Cr_2O_3, on the film surface during depth profiling by Auger electron spectroscopy (AES) analysis. The formation of the oxide layer was cited as the reason for the superior corrosion resistance. Tagami [90, 91] studied two aspects of the corrosion behaviour of r.f.-magnetron-sputtered Co-(18–26) at % Cr films. Their first study dealt with the rate and the effect on microstructure of corrosion caused by exposing the films to 85% RH at 80 °C. The rate determination and the TEM analysis of the microstructure assert that lower (< 4 mTorr) sputtering pressure and high (> 4 W cm^{-2}) power favour fine grain size and reduce segregation of chromium at grain boundaries, thus improving corrosion resistance. In the second study, Tagami and Hayashida [91] determined the corrosion rate and the associated activation energy (ΔE_c) for sputtered Co-(0–26) at % Cr films. The ΔE_c value, ranging from 0.075 eV to 0.32 eV, tends to decrease, irrespective of the Cr%, when Argon pressure is increased to 8 mTorr from 1 mTorr. They explicitly stated that corrosion resistance for the Co-22 at % Cr film is more than 10 times larger than that for Co films.

In an earlier study, Dubin *et al.* [92] studied broadly the corrosion behaviour of r.f.-diode-sputtered films of a variety of Co-based alloys, including Co-18 at % Cr and Co-20 at % Cr, exposed to corrosive environments containing H_2S, Cl_2, NO_x, or/and SO_2 with or without high RH at 79–95 °C. In general, the presence of significant amounts of water vapour (50–75 % RH at 85 °C) is necessary to produce chemical reactions and degrade the magnetic properties of the films. Simple oxidation does not occur in the absence of water vapour, and dry atmospheres prevent degradation. In terms of percentage penetration of oxygen, sulphur, or chlorine into the sample, the Co–Cr films display the best resistance to corrosive attack.

Wang and Warren [93] examined the corrosion behaviour of r.f.-sputtered Co and Co–Cr films by exposing the films to a sulphuric acid electrolyte. They confirmed the formation of a passive layer containing a chromium oxide when the Cr content exceeds 15–17%. In addition, evidence was found for the stabilization of Co oxides by the presence of Cr. AES analysis results also suggest that corrosion and passivation occur concurrently along the open spaces or crevices between columnar grains during the electrochemical exposure.

Corrosion resistance of Co–Cr films with and without carbon overcoats was investigated by Novotny *et al.* [94]. Wet oxidation of uncoated films led to preferential formation of cobalt oxide and hydroxide. Cobalt migration through the carbon overcoat was

detected at ambient conditions and at 90 °C and 90% RH. The corrosion process is thus viewed as electrochemical in nature and involving three steps: (a) dissolution of cobalt in adsorbed water, (b) migration of cobalt ions through permeable carbon, and (c) precipitation of Co-rich particles on the overcoat surface. The latter workers consequently specify that carbon overcoats for the Co–Cr recording media be nonporous, impermeable to water or metallic ions, and have low electrical conductivity in order to provide good corrosion protection for the Co alloys. They also conclude that environments with very low humidity and concentration of corrosive gases inhibit the corrosion processes in the Co–Cr alloys significantly, in agreement with the results of Dubin *et al.* [92].

The addition of a small amount (< 5 at %) of some of the lanthanides (Pr, Nd, Sm, or Gd) was found to improve the corrosion resistance of evaporated Co–Ni films substantially [95]. Inspired by the latter results, Smith *et al.* [96] substituted the Co-21 at % Cr alloy with Gd and evaluated the effect of Gd substitution on the corrosion behaviour. For small Gd concentrations, the d.c.-magnetron-sputtered films remained crystalline, but the films showed partial or complete lack of phase segregation. Films with 4 at % Gd became amorphous. Anodic polarization data showed much improved corrosion resistance for the Gd-doped Co–Cr films with Gd in the 0.4–1.7 at % range. The improvement is ascribed to an improved homogeneous microstructure.

2. Layered structures of PMA films for improved PMR performance

Early in the development of PMR media, Iwasaki *et al.* [97] demonstrated the advantages of inserting an underlayer of a soft magnetic material such as permalloy (78% Ni–Fe) between the substrate and the Co–Cr film in PMR. Layered structures such as the Co–Cr/Fe–Ni films were initially called "composite anisotropy media" [97], but they later became more widely known as double-layer (perpendicular) media [98, 99]. Further development in this field has broadened the term "layered structure" to include a host of other forms: intrinsic and extrinsic initial layers, and multilayers with or without compositional modulation. Developments of various forms of layered structures are reviewed separately.

2.1. The intrinsic initial layer (IIL)

As early as 1981, Coughlin [100], Judy *et al.* (I: [56]) reported that "a sublayer of poor orientation was observed" in r.f.-sputtered Co–Cr films with strong PMA. In 1984, Wuori and Judy [101] further revealed that the initial, 100–150 nm-thick layer of an r.f.-diode-sputtered 1 μm Co–Cr film exhibited distinctly different characteristics in (a) SEM images of the fractured cross-section, (b) in-plane hysteresis loops, and (c) rotational hysteresis torque measurements in comparison with the overall behaviour of the film. They noted that "this layer seems to reverse (the magnetization) by in-plane domain-wall motion in spite of the dominant perpendicular curling or buckling reversal of the film as a whole". Byun *et al.* [73, 74] and Niimura *et al.* [27] echoed the existence of the IIL in their later studies. The thickness of the initial layer, however, was limited to only 20 nm by Niimura *et al.*

The significance of the initial layer is twofold. First, since the layer observed by Wuori and Judy is intrinsic in nature, it is reasonable to assume that every Co–Cr film contains two layers: the initial layer with in-plane orientation, and the rest of the film with perpendicular orientation. In this sense, every Co–Cr film of sufficient thickness may be considered as a layered structure or as a double layer. Second, later studies have clearly shown that this intrinsic initial layer may be replaced by an extrinsic layer of a foreign substance for better control of the PMA properties of the subsequently deposited Co–Cr film. Howard [102] reviewed the status (up to early 1986) of the studies on the growth of the initial layer in Co–Cr films and of methods to control and improve the nucleation and growth at the substrate surface.

2.2. The extrinsic initial layer (EIL)

Based on the preceding discussion, we may define an extrinsic initial layer (EIL) as an extra film inserted between the substrate and the PMA film. The thickness of this extra film is normally less than 100 nm, and its material is in most cases a non-magnetic element such as Ti, Ge or C. It may, however, also be an alloy or an oxide or even a Co–Cr alloy of the same composition as the main PMA film. Some authors, e.g. Jeanniot and Bouchand [103] and Sakamoto *et al.* [104], called them underlayers instead of the initial layers. It was also called the nucleation layer by Schrauwen *et al.* [105], the initial growth layer by Kitakami *et al.* [106], the seed layer by Byun *et al.* [73], and the initial sublayer by Hirono and Furuya [107]. The effect of the nucleation layer on the growth and magnetic properties of Co–Cr films was extensively reviewed up to 1986 by Howard [102].

Thus far, titanium has attracted the most attention as the EIL material. Kitakami *et al.* [106] applied the evaporation–deposition process to fabricate both the Ti initial layer and the PMA film of Co–Cr on a polyimide substrate at 140 °C. The Ti layer and the Co–Cr film are 25 nm and 200–300 nm thick, respectively. Although the Ti layer does not improve the *c*-axis texture, it does increase $H_{c,\perp}$ by virtue of shape-anisotropy improvement resulting from the formation of a distinctly segregated microstructure. The increasing effect of the Ti layer on $H_{c,\perp}$ was also reported by Jeanniot and Bouchand [103], who cited an increase from 440 Oe to 635 Oe or 800 Oe, depending on whether the preferred orientation of the h.c.p. Ti layer is (0 0 2) or (1 0 0). The (1 0 0) orientation came about when a −100 V bias voltage was applied to the substrate during the sputter-deposition of Ti.

The presence of the Ti layer also narrowed the dispersion of the *c*-axis orientation in the Co–Cr film by reducing $\Delta\theta_{50}$ from 8.6° to 4.2° and 3.6° and decreased the longitudinal remanence from 42% to 18% and 15% with the (0 0 2) and (1 0 0) Ti layers,

respectively. The shift of the preferred orientation of the Ti layer from (0 0 2) to (1 0 0) is accompanied by an increase of 0.9% in the (0 0 2) d-spacing, indicating an elongation of the h.c.p. lattice along the c-axis because of the -100 V bias voltage. The latter workers concluded that the (1 0 0) preferred orientation of the Ti layer is more efficient than (0 0 2) orientation in promoting the "vertically oriented" magnetic anisotropy for Co–Cr. A pseudo-epitaxial effect was cited as the reason for the benefit of the (1 0 0)-oriented Ti layer.

The effect of the Ti layer on $H_{c,\perp}$ of the Co–Cr film was reported differently by Hirono and Furuya [107], however. In the latter work, a 30 nm Ti layer was first deposited on NaCl or surface-hardened Al substrates at 230 °C by d.c.-magnetron sputtering, followed by the deposition of Co-21.5 at% Cr by r.f.-magnetron sputtering. The $H_{c,\perp}$ of the composite film was observed to decrease "drastically" with increasing r.f.-sputtering power (P_{rf}). For example, $H_{c,\perp} = 800$ Oe at $P_{rf} = 1$ kW but decreased to 400 Oe at $P_{rf} = 4$ kW. Such pronounced dependence of $H_{c,\perp}$ on P_{rf} is viewed as highly undesirable because high P_{rf} is required in order to attain high deposition rates in the mass production of the PMR medium. Fortunately, it was found that this dependence disappears when a very thin (20–30 nm) Co–Cr "sublayer" is deposited from the same target but at lower power prior to the deposition of the final Co–Cr film.

A specific example of the latter structure involves a 30 nm Ti initial layer, a 30 nm Co-21 at % Cr layer deposited at 0.5 kW, and a 200 nm Co-21 at % Cr main layer at 4 kW for a deposition rate of 5.8 nm s^{-1}. TEM examination of the triple-layered structure reveals that the Co–Cr sublayer features a segregated microstructure that is inherited by the main film despite the large increase in subsequent sputtering power. Hirono and Furuya conclude that a segregated microstructure is essential in attaining high perpendicular coercivity.

Although the key role played by the Cr segregation in the magnetic behaviour of the PMA film is echoed by Tanaka and Masuya [108], they relate the segregation phenomenon directly to the Ti layer without the Co–Cr sublayer. Meanwhile, they cite many other beneficial effects of the Ti layer:

(1) assisting the normal alignment of the c-axis of crystals in the PMA film by means of an epitaxial-growth effect

(2) promoting the growth of columnar grains

(3) limiting the reduction of M_S with rising substrate temperature

(4) enhancing the perpendicular anisotropy constant

(5) increasing $H_{c,\perp}$

(6) improving the squareness of the perpendicular hysteresis loop.

In another study on evaporated Co–Cr films with Ti layers, Sakamoto *et al.* [104] also observed the promotion of the columnar grains growing directly from the Ti layer throughout the thickness of the Co–Cr film.

Two studies were conducted on the effect of Ge initial layers. Futamoto *et al.* [109] examined the effect of a host of materials in 30 nm initial layers on the dispersion of the c-axis orientation of the Co–Cr films. Both the initial layer and the main film were deposited by the evaporation process. Tests were conducted on 20 elements (Al, Si, Sc, Ti, V, Cr, Ni, Ge, Y, Zr, Nb, Ru, Rh, Pd, Sn, Sb, Hf, Re, Pt, Bi) and 5 oxides (MgO, Al_2O_3, SiO_2, TiO, ZnO). The extensive survey found the amorphous-like Ge and (to a much lesser extent) Ti, Si, and perhaps Sc to be suitable underlayer materials for the enhancement of the preferred perpendicular orientation of columnar grains in the Co–Cr films. Cross-sectional TEM studies indicate that the Co–Cr films formed on the Ge underlayer featured pillar-like columnar grains grown vertically throughout the film thickness and had a strong PMA.

The read–write characteristics have been improved by the presence of the Ge layer and a very high recording density of $D_{50} = 230$ kiloflux change per inch attained. The effect of the Ge layer was further examined by Schrauwen *et al.* [105]. Rather thick (350 nm) Ge layers and Co-21 at % Cr films with varying thickness (10–800 nm) were fabricated on 14.5 μm polyester (PET) substrates at 30 °C by r.f. sputtering. The Ge underlayer promotes the perpendicular anisotropy of the Co–Cr film, provided the Ge layer thickness exceeds a critical value of about 200 nm. The minimum thickness of the Ge initial layer is required to effectively seal the PET substrates. The layered Co–Cr/Ge films also show low coercivity (126–377 Oe) and a fine columnar structure with column widths of 30–50 μm.

The effect of carbon was studied by several workers. Tsumita *et al.* [45] found that deposition of a 5 nm-thick carbon layer on the amorphous Co–Zr–Mo underlayer would further improve the c-axis normal orientation of the Co–Cr film. Niimura *et al.* [27, 110] inserted carbon as the intermediate layer between 200 nm Co–Cr films in a multilayered structure and found that the presence of carbon tended to promote fine spherical grains in the Co–Cr films, leading to a well-oriented c-axis in the film normal direction and strong PMA. The effect of the Co–oxide initial layer was found by Byun *et al.* [73] to increase the first PMA constant K_1 by 40% and to decrease the $\Delta\theta_{50}$ by as much as 75%. The results were interpreted in terms of the role played by the Co–oxide as seeds or nucleation sites having [1 1 1] orientation perpendicular to the substrate. The CoO seeds enhance the growth of the h.c.p. phase of Co–Cr with the preferred c-axis orientation and minimize the thickness of the transition layer between the film and the substrate.

2.3. The double-layer structure with a soft magnetic underlayer

At the outset of Section 2, we mentioned that Iwasaki *et al.* conceived the idea of using a soft magnetic material to support the PMA film to constitute a double-layer medium in a 1979 study [97]. They demonstrated two functions of the Ni–Fe underlayer in the perpendicular recording:

(1) to reduce the magnetic reluctance of the air gap in the perpendicular head, thereby reducing the ampli-

tude of recording current for PMR; moreover, from the reciprocity theorem, the reproducing sensitivity of the head should also be improved;

(2) to rotate the magnetization vector to establish a horseshoe-type magnetization mode (I:[3]) in the medium, thus reducing the demagnetizing field; this would then enable the remanent magnetization to increase.

The spin alignment in the two layers of a typical double-layer medium is shown in Fig. 29a, and the effect of the Ni–Fe underlayer in perpendicular recording in Fig. 29b. Note in the latter figure that a part of the magnetic path is made through the underlayer for the flux induced by the auxiliary pole. In the early fabrication, a typical double-layer medium would consist of a 0.5 μm-thick 78% Ni–22% Fe permalloy film and a 1 μm-thick Co–Cr film, with both films having M_s in the 500–600 e.m.u. cm^{-3} range. Besides the basic difference in the anisotropy mode, the two films also show vast difference in the microstructure: lack of preferential growth in the f.c.c. permalloy layer and well-developed columnar grains with the *c*-axis of the h.c.p. phase of Co–Cr aligned in the film normal. These microstructures are consistent with the different magnetic functions served by the two layers–high permeability for the improvement of recording sensitivity in a supporting role by the underlayer, perpendicular magnetizability in a major role for PMR by the Co–Cr layer.

In a later study [98], Ouchi and Iwasaki confirmed that the optimal thickness of the soft magnetic underlayer is ~ 0.5 μm. Beyond this thickness, the recording output decreases and there is no gain on the recording sensitivity, which is also reduced by an excessive thickness of the Co–Cr layer. These effects are ascribed to the non-linear magnetic behaviour of the underlayer and the weakened interaction between the main pole and the underlayer. Other aspects of the Ni–Fe underlayer were investigated by many workers:

1. [103] on the optimization of the sputtering conditions for the preparation of the 80% Ni–Fe permalloy layer, by Jeanniot and Bouchand.

2. [111] furnishing evidence for epitaxial growth of Co–Cr on permalloy, by Simpson *et al.* The angle-of-incidence effects were examined and explained by a theory combining the absorption phenomenon and the canting, or turning, of the (1 1 1) planes of the permalloy film and the (0 0 0 2) planes of the Co–Cr film from the film normal toward the direction of the substrate motion during sputtering. The canting phenomenon was further examined through X-ray depth profiling in a follow-up study [112].

3. [113] on the assessment of the magnetic properties of Co–Cr films with and without Ni–Fe underlayers by Stam *et al.* The assessment involved FMR and VSM measurements. More FMR measurements were conducted later [114] on both double-layer films and a single Co–Cr film. Several resonance curves were observed for Co–Cr, implying magnetic stratification of the Co–Cr film into several sublayers.

4. [115] dealing with the effect of inserting a titanium layer between the Ni–Fe underlayer and the Co–Cr film in an evaporated double-layer structure on the in-plane coercivity of the Ni–Fe layer, M_s and $H_{c,\perp}$ of the Co–Cr film, recording output voltage, recording sensitivity, and the overwrite signal/noise ratio, by Tanaka *et al.* For all these properties, the effect of the Ti interlayer are favourable.

5. [116] reporting high $H_{c,\perp}$ values (> 2000 Oe) for double-layer films having an unusual thickness ratio (2 μm for Fe–Ni/0.15 μm for Co–Cr), a 0.02 μm Ti layer between glass substrate and the permalloy underlayer, and a 0.02 μm Ti layer between the permalloy underlayer and the Co–Cr film, by Kiuchi *et al.* The development of such multilayers was for "high-energy" PMR medium on a rigid disk.

Several other soft magnetic materials were used in place of permalloy. One substitute material is the mumetal, which is composed of 77% Ni–14% Fe–5% Cu–4% Mo in this case [117]. This composition is closely related to 78-permalloy (78% Ni–Fe) in the nickel content but adds copper and molybdenum at the expense of iron. Reasons for using the mumetal were not given by Buttafava *et al.* [117] and Parker

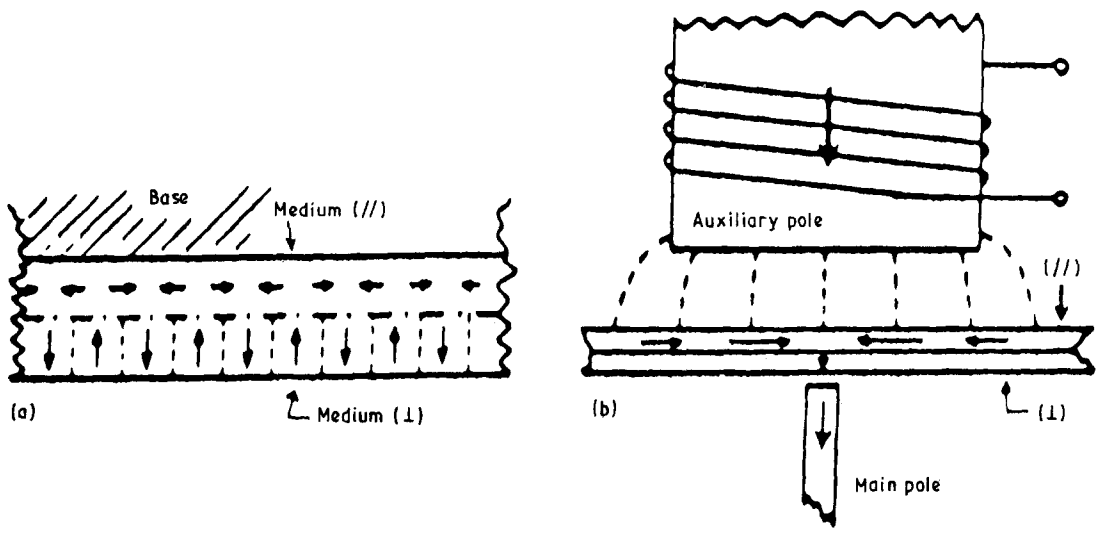

Figure 29 (a) Remanent-state spin alignment in the Fe–Ni and Co–Cr films. (b) Effect of the Fe–Ni layer on flux distribution through the auxiliary pole of a SPT head system in the perpendicular recording process [97].

[118]. Both studies indicate the suitability of the mumetal as an underlayer material.

Another substitute material is the Co–Cr alloy whose Cr content differs from that of the PMA film. Kouchiyama *et al.* [119] purposely varied the Cr% in order to evaluate its effect on $H_{c,\perp}$ and H_k of the double-layer film. These two properties show opposite dependencies on the Cr% in the underlayer. The grain orientation of the PMA film is also affected.

Iron [98, 120] was also used to substitute permalloy in the underlayer. Fukizawa and Naoe [120] chose iron for its high M_s ($4\pi M_s$ up to 21.5 kG) and low coercive force (3.5 Oe), provided the underlayer was deposited under proper sputtering conditions. Moreover, to improve corrosion resistance, the argon gas pressure and the bias voltage must be optimized critically in order to eliminate residual stresses in the Fe film. The quality of the *c*-axis orientation of the Co–Cr film was found to depend sensitively on the degree of the (1 1 0) texture in the Fe film.

Bernards *et al.* [121] also tried the sputtered amorphous underlayer of the Co-4.8 at % Zr-8.8 at % Nb alloy together with two intermediate-layer materials deposited on the underlayer: Ti (crystalline) and Ge (amorphous). In the case of the Ni–Fe underlayer, the combination of a Ti intermediate layer and bias sputtering of the Ni–Fe resulted in well-oriented Co–Cr layers with high $H_{c,\perp}$ and low $H_{c,//}$ in the Ni–Fe underlayer. The presence of a Ge intermediate layer in the Co–Cr/Co–Zr–Nb double layer also improves the *c*-axis orientation of the Co–Cr film with lower $H_{c,\perp}$ values compared with those when using the Ti intermediate layer. Recording media involving these modified double layers were characterized in terms of medium noise and probe-head efficiency.

The recording performance of various double-layered media was evaluated in different terms. In media consisting of Co–Cr films with Cu–Mo permalloy or pure iron underlayers, Ouchi and Iwasaki [98] determined the dependence of recording and reproducing sensitivities on the underlayer thickness and on the ratio of the saturation flux of underlayer and the main pole of the recording head. Some of the results have been discussed earlier. Other studies of the double-layer media for PMR include:

1. [99] on the role played by M_s of the underlayer in the shape and magnitude of the calculated write field, by Luitjens *et al.*

2. [122] on the dependence of the readback signal upon the anisotropic permeability and thickness of the underlayer, by Simpson *et al.*

3. [123] on the relationship between the recording noise output and $H_{c,\perp}$ of the permalloy underlayer, by Luitjens *et al.*

4. [124] using a one-sided probe-head to attain high-density recording, by Zieren *et al.* The recording features are compared with those performed by a ring head.

5. [125] involves theoretical analyses in which numerical boundary integral methods are used to compute the pulse and frequency response of asymmetric thin-film heads and double-layer perpendicular recording films. An implicit dependence on spacing between head and sublayer and non-classical thickness factors are revealed. The calculated results agree closely with the experimental data.

Finally a special study of the double-layer structure was conducted by Maloney [126]. Instead of depositing the Co–Cr alloy in a single layer, Cr and Co films with thicknesses of 300–600 nm and 10–50 nm, respectively, are deposited separately on Al or Pyrex substrates. Such double-layer media show flexibility in the variation of coercivity and remanence–thickness product and give better recording performance than "standard particulate disks". For perpendicular recording, however, this approach offers no particular attraction compared to media containing alloy films.

2.4. The multilayer structure

Robinson [127] attempted to construct multilayered media for perpendicular recording by depositing alternate layers of non-magnetic $(Co_{85}Cr_{15})_{70}Ta_{30}$ and magnetic $(Co_{85}Cr_{15})_{90}Ta_{10}$ on polyimide substrates. By changing the layer thickness, perpendicular and longitudinal coercivities and M_s of the magnetic layers can be varied widely so that the first magnetic layer can act as a soft magnetic film like the permalloy. Another advantage of this approach is that the composition of the multilayers can be easily changed by varying the d.c. power input of, and hence the sputtering rate from, the Ta target while the other target of the $Co_{85}Cr_{15}$ alloy is sputtered at a constant power input.

Walmsley *et al.* [128] fabricated multilayered films of alternate layers of Cr and Co by d.c.-triode and d.c.-magnetron sputtering, respectively. The film thickness varied from 2.5 to 10 nm, and the number of layers varied from 60 to 344. The results were scientifically interesting because stable b.c.c. phase of the Co was detected with a magnetic moment close to that of the normal hexagonal phase.

3. Assessment and future developments

3.1. Prospect of PMR and future development in perpendicular recording media

Although the application of PMA films for high-density magnetic recording is not our main concern here, this review would be incomplete if we left the future of the films entirely undiscussed. The impetus of the great, concerted effort in the fabrication and characterization of Co–Cr films we have witnessed in the past decade is to develop a new, promising technology for high-resolution [129], high-density magnetic recording of information that would surpass the ultimate capability of conventional longitudinal magnetic recording.

The application prospect of PMA films and the future of PMR have been reviewed and predicted almost yearly since 1984 by prominent researchers, notably Iwasaki [130, 132], Suzuki [133], Mallinson [134], Hatakeyama [135], Nakamura and Tagawa [136], Hokkyo [137], and Ouchi [131, 132, 138]. For an emerging, fast-moving technology such as PMR, the value of each review is limited to three or four

years. It is therefore futile to go through all these reviews, many of which are already more than four years old and whose predictions are now obsolete or out of date. For example, Mallinson [134] stated in his 1985 review paper that "for in-contact operation, it appears that 300×10^6 bits per square inch ($= 4.65 \times 10^5$ bits mm^{-2}) will prove feasible". The projected density for PMR in 1988 by Nakamura and Tagawa [288] is more than 860 times as great at 4×10^8 bits mm^{-2}.

To be consistent with what we set out to do in this review, we will focus our discussion in this section on a 1988 paper modestly entitled, "Possibilities of Perpendicular Magnetic Recording" by Nakamura and Tagawa [136]. In their work, the potential of PMR was theoretically analysed by computer simulation for the combined operation of a single-pole head and a double-layer medium. It is shown that, in PMR, the perpendicular magnetization mode is maintained even though the linear bit density exceeds 570 kFRPI. Therefore the demagnetizing loss due to the change of magnetization mode from semicircular to circular shape that occurs in the longitudinal recording is eliminated. High resolution is revealed for PMR where a single bit size approaches several diameters of the submicrometre-size grains of the Co–Cr film. The simulated capability of PMR is plotted in terms of linear and areal bit densities against track density in Fig. 30 together with those of the various (rigid- and flexible-disk systems and video-cassette tape systems) conventional longitudinal recording modes and the thermomagnetic-optical method. It is gratifying to note in the figure that the potential areal bit density of PMR at $> 4 \times 10^8$ bits mm^{-2} is at least two orders of magnitude higher than that of thermomagnetic-optical recording, which competes fiercely with PMR as the next generation of information recording technology to replace the conventional particulate process. This is partly because, in optical recording, high areal density is achievable up to the bit area corresponding to a beam diameter [136]. Hence a sophisticated laser diode that can emit a short wavelength to attain the targeted density at around 2×10^6 bits mm^{-2} is needed.

To realize the great potential of PMR, Nakamura and Tagawa cautioned that the Co–Cr media must be more reliable and the recording head must be more sensitive and efficient. The reliability of the media refers largely to their durability for the eventual in-contact medium-head operation. This in turn necessitates higher wear resistance and better surface finish of the media. The efficiency of the head refers to the magnetic flux leakage from the main pole of the head to the other side of an auxiliary yoke. According to Yamamoto *et al.* [139], the flux-leakage efficiency of various types of single-pole heads at present is still very low: 7% for auxiliary-pole-driven type [140], 15% for single-sided main-pole-driven type [141–143], and 45% for asymmetric thin-film type [144]. If the single-pole thin-film head is constructed of the symmetric type, the efficiency could be increased to about 90% [139]. This type should also improve sensitivity of the head by increasing the normalized reproduced voltage from the current level of 0.05 [145] to $0.3_n V_{o\text{-}p}/(\mathrm{T\,m\,s^{-1}\,nm})$ [136]. The choice of the head remains unsettled since the ring type has recently redrawn the attention of Iwasaki and Ouchi [146] and Suzuki *et al.* [147]. Although the problems associated with the head and its interaction with the medium are not our main concern here, their importance in the future of applying PMA films for high-density magnetic recording should not be overemphasized.

Progress has been made in the improvement of wear resistance of the Co–Cr media. Previous discussion has cited that Furuya *et al.* [83], Kurokawa *et al.* [87], and Nagao *et al.* [88] subjected various Co–Cr films to durability tests in excess of ten million passes successfully. Also, effective lubrication has been demonstrated to reduce friction and prolong wear life of the media by Buttafava *et al.* [85]. Ouchi and Iwasaki [132] disclosed two factors that seriously affect the

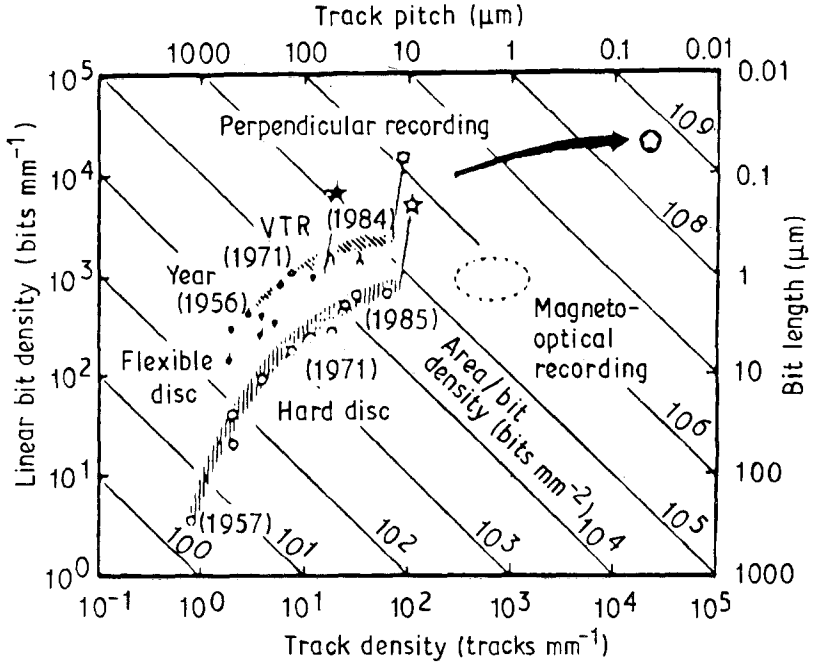

Figure 30 Projected capability of perpendicular magnetic recording in comparison with capabilities of other recording methods and modes [136].

durability of the media: (a) dust on the surfaces of media (and heads) and (b) defects like nodules on the medium surface (I:[130]). These factors have not received adequate attention until recently. Remedial measures to alleviate the effect of these factors are (a) fabricating media and heads in clean-room environments, (b) carefully selecting a polymeric substrate whose thermal expansion coefficient and Young's modulus are close to those of the metallic layers, and (c) thorough cleaning and degreasing of the substrates [136].

3.2. State-of-the-art of the science and technology of the fabrication of PMR media

The foregoing review of 300 papers (out of a total of approximately 1000 publications [138]) has clearly shown that the intensive work on PMA films in the past 12 years has developed the science and technology of this class of films to such an extent that high-density, high-resolution PMR is now a reality. Many options are open for the selection of the most efficient methods for film and medium fabrication. Moreover, the optimal conditions for the operation of these methods to yield desirable qualities of the PMA films, their underlayers, and protective coatings have been established. The films have been characterized so broadly that their outstanding magnetic properties as well as their inherent deficiencies have been exposed and improved or remedied. It is reasonable to state that a solid foundation has been laid out for PMR technology, whose application is merely a matter of time.

Under these circumstances, it is worthwhile to delineate the status and state-of-the-art of the science and technology of PMA films and PMR media. The delineations also will serve as the concluding remarks of this lengthy review.

3.2.1. Materials for PMA films

It is both gratifying and ironic to note that Co–Cr alloys are still the best materials for PMR. The gratification mainly refers to the original proposal of Iwasaki (I:[44]) who suggested the Co–Cr alloys as the most attractive system for PMA films. His suggestion was derived from the (hexagonal) crystal structure, the (uniaxial) magnetic anisotropy, and the ease with which the M_s and $H_{k,\perp}$ could be varied with the Cr content. The irony stems from the fact that numerous other materials have been tried but failed to replace the Co–Cr alloys. Indeed, Co–Cr alloys still display the largest perpendicular anisotropy and the best overall value combining magnetic properties, adaptability to stringent fabrication conditions, and wear and corrosion resistances.

There are areas in which the composition of the binary Co–Cr alloys could be modified for property improvements in the film and medium, however. For instance, the doping of 0.4–1.7 at % Gd [56] or Mo [139] improves corrosion resistance significantly. The addition of a small amount of Zr (0.5 at%), Ta [140], or 5% W and 1% C [303] improves wear resistance, thereby prolonging the medium life. To make the Co–Cr films more flexible, the dissolution of Zn (< 1 at %) or Cu (2 at %) is adopted to reduce Young's modulus of the film by 50% [142]. If the formation of the intrinsic initial layer is an important avenue to strengthen the PMA film and to enhance the PMR performance, the addition of Nb proves to be effective [143].

3.2.2. Properties of PMA films required for PMR

After satisfying the basic condition for the onset of PMA expressed by Equation 1A or 1B in Part I, the saturation magnetization of the chosen Co–Cr alloy should exhibit as high M_s as possible in the film to ensure strong magnetic interaction between the recording head and medium. This is especially true when a single-pole-type head is used. This in turn necessitates a high packing density in the film. Perpendicular coercivity of the film is now preferred to exceed 1000 Oe in order to maximize the output voltage, provided the recording head is capable of producing sufficient field strength. For different reasons [138], both SPT and ring heads favour this high $H_{c,\perp}$ requirement. The microstructure of the PMA film should have columnar grains as fine as possible to promote the recording density. Also, the columns should grow straight up from the bottom to the top without crystal defects, and their c-axis orientation should be as sharp as possible.

Equally important is the wear resistance of media. We now expect each medium to withstand at least 10 million passes without noticeable loss of the output voltage and change in the signal/noise ratio. Many means are devised to improve the mechanical strength of the Co–Cr film such as alloying with Ta, Zr, or W-C, covering the medium surface with diamond-like carbon deposition, and reducing friction by using fluid lubricant. Lately attention has been directed to the quality and surface conditions of the polyimide and other polymeric substrates and to the surface finish of the medium and solutions to the problems.

3.2.3. Methods for film preparation

Sputtering and electron-beam evaporation processes are efficient for the preparation of Co–Cr films having excellent qualities. By far, however, sputtering has been the most popular process by virtue of its versatility (I:[53]), the superior qualities (e.g. lower $\Delta\theta_{50}$) of the films it produces, and the absence of complications caused by differential rates of evaporation between Co and Cr. The inherent disadvantage of the sputtering process–low rates of deposition–can be remedied by the special techniques discussed in Section 4.1.4 in Part I, notably the FTS method (I:[61, 67]), the IPT/F targets (I:[69]), and the exposed-pole magnetron process [154]. For mass production of PMR media, the roll-coater system (I:[75, 81]) is valuable. Ouchi [148] recently commented that the Co–Ni–Re–P films prepared by the electrodeposition

method with anodic oxidation (I:[99]) offer two advantages: (1) they yield rigid-disk media whose PMR performances are good, and (2) they can be operated in room atmosphere, thus making the fabrication process convenient and less expensive.

3.2.4. Design of recording media

The structure design of a PMR medium should be varied according to the type of recording head. Two types of heads, the single-pole type (SPT) and the conventional ring type, have been tried with mixed results [148]. SPT is further diversified into main-pole and auxiliary-pole excitation. The latter is the best system with regard to perpendicular field purity. For the SPT head, the medium should have a double-layer structure with a soft magnetic backup layer [97]. For better PMR performance with respect to medium noise and recording resolution and to attain recording densities up to 100 kFRPI, the PMA film thickness should be kept small, around 0.1 μm; also, the main pole thickness and the spacing between head and medium should be kept to a minimum.

One design of the medium used in conjunction with the ring head is a single Co–Cr film without the backup layer. This single-film medium-ring head combination has the disadvantages that the reproduced pulse has a dipulse shape and its overwrite is worse than that produced by the double-layer medium and SPT head combination. To alleviate these problems, a thin (20 nm), soft magnetic layer is recommended [146]. To increase H_k for high output voltage by improving the *c*-axis orientation, a thin (30 nm) initial layer of Ge [109], Ti [106], or CoO [73] inserted underneath the PMA film is also recommended.

At present, the development of the recording head lags behind that of PMR media. This situation, coupled with the close tie between the medium and the head, is partly responsible for the delay of PMR application.

Acknowledgements

I am indebted to H. Awano, M. Futamoto, S. Honda, F. Kugiya, D. E. Laughlin, H. Masuva, and M. Shiraki for furnishing glossy prints of their original photomicrographs. Thanks are due to D. Makowiecki for his support of this work and to J. Kass and A. Jankowski for their financial assistance. The work was performed under the auspices of the US Department of Energy by the Lawrence Livermore National Laboratory under contract W-7405-Eng-48.

References

1. W. G. HAINES, *IEEE Trans. Magn.* **MAG-20** (1984) 812.
2. P. V. MITCHELL, A. LAYADI, N. S. VANDERVEN and J. O. ARTMAN, *J. Appl. Phys.* **57** (1985) 3976.
3. P. V. MITCHELL, A. LAYADI, K. MOUNTFIELD, C. HWANG, J. E. SNYDER and J. O. ARTMAN, *J. Magn. and Magn. Mater.* **54–57** (1986) 1701.
4. B. L. RAMAKRISHNA, C. H. LEE, Y. CHENG and M. B. STERNS, *J. Appl. Phys.* **61** (1987) 4290.
5. M. L. COFIELD, D. GLOCKER and J. S. GAU, *J. Appl. Phys.* **61** (1987) 3810.
6. K. YOSHIDA, T. OKUWAKI, N. OSAKABE, H. TANABE, Y. HORIUCHI, T. MATSUDA, K. SHINAGAWA, A. TONOMURA and H. FUJIWARA, *IEEE Trans. Magn.* **MAG-19** (1983) 1600.
7. K. YOSHIDA, Y. HONDA, T. KAWASAKI, M. LOIZUMI, F. KUGIYA, M. FUTAMOTO and A. TONOMURA, *IEEE Trans. Magn.* **MAG-23** (1987) 2073.
8. R. S. INDECK and J. H. JUDY, *IEEE Trans. Magn.* **MAG-20** (1984) 730.
9. D. K. LOTTIS and E. D. DAHLBERG, *J. Appl. Phys.* **63** (1988) 2920.
10. K. KABAYASHI and G. ISHIDA, *J. Appl. Phys.* **52** (1981) 2453.
11. W. G. HAINES, *J. Appl. Phys.* **55** (1984) 2263.
12. Y. FUJII, K. TSUTSUMI, T. NUMATA and Y. SAKURAI, *J. Appl. Phys.* **55** (1984) 2266.
13. Y. UCHIYAMA, K. ISHIBASHI, H. SATO, U. HWANG and T. SUZUKI, *IEEE Trans. Magn.* **MAG-23** (1987) 2058.
14. Y. MAEDA, M. ASAHI and M. SEKI, *Jpn. J. Appl. Phys.* **25** (1986) L668.
15. J. E. SNYDER, K. R. MOUNTFIELD and M. H. KRYDER, *J. Appl. Phys.* **61** (1987) 3146.
16. J. W. SMITS, S. B. LUITJENS and F. J. A. DEN BROEDER, *J. Appl. Phys.* **55** (1984) 2260.
17. Y. NAKAMURA and S.-I. IWASAKI, *IEEE Trans. Magn.* **MAG-23** (1987) 153.
18. S. B. OSEROFF, D. CLARK, S. SCHULTZ and S. SHTRIKMAN, *IEEE Trans. Magn.* **MAG-21** (1985) 1495.
19. B. C. WEBB, S. SCHULTZ and S. B. OSEROFF, *J. Appl. Phys.* **63** (1988) 2923.
20. Y. HOSHI, M. SATSUOKA, M. NAOE and S. YAMANAKA, *IEEE Trans. Magn.* **MAG-20** (1984) 797.
21. P. BERNSTEIN, J. DESSERRE, D. JEANNIOT, O. GUEUGNON and M. PORTE, *IEEE Trans. Magn.* **MAG-20** (1984) 809.
22. S. HONDA and T. KUSUDA, *IEEE Trans. Magn.* **MAG-21** (1985) 1444.
23. J. O. ARTMAN, *J. Appl. Phys.* **61** (1987) 3137.
24. H. MIYAJIMA, K. SATO and T. MATSUDA, Proceedings of the Seventh Annual Conference on Magnetics, Japan (1975) 5pB-13 (in Japanese).
25. K. ISHIBASHI, Y. UCHIYAMA, U. HWANG and T. SUZUKI, *J. Appl. Phys.* **63** (1988) 2914.
26. Y. NIIMURA, S. NAKAGAWA, Y. KITAMOTO and M. NAOE, *J. Appl. Phys.* **61** (1987) 3152.
27. Y. NIIMURA, S. NAKAGAWA, Y. HOSHI and M. NAOE, *IEEE Trans. Magn.* **MAG-23** (1987) 2461.
28. J. R. DESSERRE and D. JEANNIOT, *J. Appl. Phys.* **54** (1983) 2820; *IEEE Trans. Magn.* **MAG-19** (1983) 1647.
29. K. TAGAMI, H. GOKAN and M. MUKAINARU, *IEEE Trans. Magn.* **MAG-24** (1988) 2344.
30. P. V. MITCHELL, K. R. MOUNTFIELD, A. LAYADI, J. E. SNYDER and J. O. ARTMAN, *IEEE Trans. Magn.* **MAG-22** (1986) 1173.
31. P. V. MITCHELL, K. R. MOUNTFIELD and J. O. ARTMAN, *J. Appl. Phys.* **63** (1988) 2917.
32. Y. NIIMURA and M. NAOE, *IEEE Trans. Magn.* **MAG-21** (1985) 1447.
33. E. KLOKHOLM, *IEEE Trans. Magn.* **MAG-12** (1976) 819.
34. T. WIELINGA, J. C. LODDER and J. WORST, *IEEE Trans. Magn.* **MAG-18** (1982) 1107.
35. R. LUDWIG, K. KASTNER, R. KUKLA and M. MAYR, *IEEE Trans. Magn.* **MAG-23** (1987) 94.
36. C. D. WRIGHT and B. K. MIDDLETON, *IEEE Trans. Magn.* **MAG-21** (1985) 1398.
37. K. ROLL, K. H. SCHULLER and W. D. MUNG, *IEEE Trans. Magn.* **MAG-20** (1984) 771.
38. J. P. C. BERNARDS, C. P. G. SCHRAUWEN, S. B. LUITJENS, V. ZIEREN and R. W. de BIE, *IEEE Trans. Magn.* **MAG-23** (1987) 125.
39. S. NAKAGAWA, M. SUMIDE, Y. KITAMOTO, Y. NIIMURA and M. NAOE, *J. Appl. Phys.* **63** (1988) 2911.
40. J. W. SMITS, S. B. LUITJENS and R. W. J. GEUSKENS, *IEEE Trans. Magn.* **MAG-20** (1984) 60.
41. K. HEMMES, J. C. LODDER and Th. J. A. POPMA, *IEEE Trans. Magn.* **MAG-23** (1987) 150.

42. D. P. RAVIPATI and W. G. HAINES, *J. Appl. Phys.* **61** (1987) 3149.
43. Y. NIIMURA, S. NAKAGAWA and M. NAOE, *IEEE Trans. Magn.* **MAG-23** (1987) 68.
44. K. OUCHI and S.-I. IWASAKI, *J. Appl. Phys.* **57** (1985) 4013.
45. N. TSUMITA, Y. SHIROISHI, H. SUZUKI, T. OHNO and Y. UESAKA, *J. Appl. Phys.* **61** (1987) 3143.
46. K. OUCHI and S.-I. IWASAKI, *IEEE Trans. Magn.* **MAG-23** (1987) 2070.
47. See, for example, US Inc. Installation Manual for US Gun II (1988) p. 8.
48. M. SAGOI and R. NISHIKAWA, *J. Vac. Sci. Technol.* **A7** (1989) 166.
49. J. C. LODDER, D. WIND, Th. J. A. POPMA and A. HUBERT, *IEEE Trans. Magn.* **MAG-23** (1987) 2055.
50. K. NISHIMOTO, in "Recent magnetics for electronics", Vol. 15 (Ohmsha and North-Holland, Tokyo, 1984) p. 29.
51. Y. HONDA, M. FUTAMOTO, T. KAWASAKI, K. YOSHIDA, M. KOIZUMI, F. KUGIYA and A. TONOMURA, *Jpn. J. Appl. Phys.* **26** (1988) L-923.
52. S. HONDA, K. TAKAHASHI and T. KUSUDA, *Jpn. J. Appl. Phys.* **26** (1987) L-593.
53. K. OUCHI and S.-I. IWASAKI, *IEEE Trans. Magn.* **MAG-18** (1982) 1110.
54. M. OHKOSHI and T. KUSUDA, *Jpn. J. Appl. Phys.* **22** (1983) L-130.
55. H. HOFFMANN, *IEEE Trans. Magn.* **MAG-22** (1986) 472.
56. L.-W. LEE, B. G. DEMCZYK, K. B. MOUNTFIELD and D. E. LAUGHLIN, *J. Appl. Phys.* **63** (1988) 2905.
57. P. J. GRUNDY, M. ALI and C. A. FAUNCE, *IEEE Trans. Magn.* **MAG-20** (1984) 794.
58. K. GOTO, T. SAKURAI and O. KITAKAMI, *Jpn. J. Appl. Phys.* **25** (1986) 1358.
59. F. SCHMIDT, W. RAVE and A. HUBERT, *IEEE Trans. Magn.* **MAG-21** (1985) 1596.
60. F. SCHMIDT and A. HUBERT, *J. Magn. and Magn. Mater.* **61** (1986) 307.
61. R. H. WADE, *Phil. Mag.* **10** (1966) 49.
62. M. OHKOSHI, H. TOBA, S. HONDA and T. KUSUDA, *J. Magn. and Magn. Mater.* **35** (1983) 266.
63. A. H. BOBECK, *Bell Syst. Technol. J.* **46** (1967) 1901.
64. M. ALI and P. J. GRUNDY, *IEEE Trans. Magn.* **MAG-19** (1983) 1643.
65. P. J. GRUNDY and M. ALI, *J. Magn. and Magn. Mater.* **40** (1983) 154.
66. F. KUGIYA, M. KOIZUMI, F. KANNO, M. SUZUKI, Y. HONDA, M. FUTAMOTO and K. YOSHIDA, *IEEE Trans. Magn.* **MAG-23** (1987) 2362.
67. T. WIELINGA and J. C. LODDER, *Phys. Status Solidi* **(a)96** (1986) 255.
68. C.-R. CHANG and D. R. FREDKIN, *IEEE Trans. Magn.* **MAG-23** (1987) 2052.
69. S. HONDA and K. TAKAHASHI, *Jpn. J. Appl. Phys.* **27** (1988) 2278.
70. J. C. LODDER, D. WIND, G. E. v. DORSSEN, Th. J. A. POPMA and A. HUBERT, *IEEE Trans. Magn.* **MAG-23** (1987) 214.
71. C. BYUN, J. M. SIVERTSEN and J. H. JUDY, *IEEE Trans. Magn.* **MAG-22** (1986) 1155.
72. K. OUCHI and S.-I. IWASAKI, *IEEE Trans. Magn.* **MAG-23** (1987) 180.
73. C. BYUN, E. M. SIMPSON, J. M. SIVERTSEN and J. H. JUDY, *IEEE Trans. Magn.* **MAG-21** (1985) 1453.
74. C. BYUN, J. M. SIVERTSEN and J. H. JUDY, *J. Appl. Phys.* **57** (1985) 3997.
75. E. C. STONER and E. P. WOHLFARTH, *Phil. Trans. R. Soc.* **240** (1948) 599.
76. S. STRIKMAN and D. TREVES, *J. Physique et Radium* **20** (1959) 286.
77. C.-Z. LI and J. C. LODDER, *IEEE Trans. Magn.* **MAG-23** (1987) 2260.
78. G. HERZER, W. FERNENGEL and E. ADLER, *J. Magn. and Magn. Mater.* **58** (1986) 48.
79. J.-G. ZHU and H. N. BERTRAM, *J. Appl. Phys.* **66** (1989) 1291.
80. Y. MOTOMURA and K. TAGAMI, *IEEE Trans. Magn.* **MAG-22** (1986) 348.
81. H. CZICHOS, in "Tribology – a systems approach to the science and technology of friction, lubrication and wear" (Elsevier, Amsterdam and New York, 1978).
82. M. YAMAURA, T. YATABE, H. MATSUZAWA, S. KODOKURA and S. SOBAJIMA, *IEEE Trans. Magn.* **MAG-22** (1986) 349.
83. N. FURUYA and Y. NAKAYAMA, *IEEE Trans. Magn.* **MAG-23** (1987) 2401.
84. S. KADOKURA, K. KAMEI, K. TERANISHI and S. SOBAJIMA, *IEEE Trans. Magn.* **MAG-23** (1987) 2404.
85. P. BUTTAFAVA, V. BRETTI, G. CIARDIELLO, M. PIANO, G. CAPORIECIO and A. M. SCARATI, *IEEE Trans. Magn.* **MAG-21** (1985) 1533.
86. H.-C. TSAI and D. B. BOGY, *J. Vac. Sci. Technol.* **A5** (1987) 3287.
87. H. KUROKAWA, T. MITANI and T. YONEZAWA, *IEEE Trans. Magn.* **MAG-23** (1987) 2410.
88. M. NAGAO, K. SANO, M. KOJIMA, H. IWASAKI, A. NAHARA and T. KITAMOTO, *IEEE Trans. Magn.* **MAG-23** (1987) 2395.
89. S. HONDA, N. YAMASHITA, M. OHKOSHI and T. KUSUDA, *IEEE Trans. Magn.* **MAG-20** (1984) 791.
90. K. TAGAMI, *IEEE Trans. Magn.* **MAG-21** (1985) 1435.
91. K. TAGAMI and H. HAYASHIDA, *IEEE Trans. Magn.* **MAG-23** (1987) 3648.
92. R. R. DUBIN, K. D. WINN, L. P. DAVIS and R. A. CUTLER, *J. Appl. Phys.* **53** (1982) 2579.
93. T. G. WANG and G. W. WARREN, *IEEE Trans. Magn.* **MAG-22** (1986) 340.
94. V. NOVOTNY, G. ITNYRE, A. HOMOLA and L. FRANCO, *IEEE Trans. Magn.* **MAG-23** (1987) 3645.
95. J. TADA, M. AKIHIRO, K. TAKEI, T. SATOH and T. SUZUKI, *IEEE Trans. Magn.* **MAG-22** (1986) 343.
96. M. G. SMITH, F. T. PARKER and H. OESTERREICHER, *IEEE Trans. Magn.* **MAG-24** (1988) 1823.
97. S.-I. IWASAKI, K. NAKAMURA and K. OUCHI, *IEEE Trans. Magn.* **MAG-15** (1979) 1456.
98. K. OUCHI and S.-I. IWASAKI, *IEEE Trans. Magn.* **MAG-20** (1984) 99.
99. S. B. LUITJENS, J. W. SMITS and V. ZIEREN, *IEEE Trans. Magn.* **MAG-20** (1984) 724.
100. T. M. COUGHLIN, M.S. thesis, University of Minnesota (1980).
101. E. WUORI and J. H. JUDY, *IEEE Trans. Magn.* **MAG-20** (1984) 774.
102. J. K. HOWARD, *J. Vac. Sci. Technol.* **A4** (1986) 19.
103. D. JEANNIOT and J. C. BOUCHAND, *IEEE Trans. Magn.* **MAG-24** (1988) 2356.
104. Y. SAKAMOTO, K. HONDA, T. NAMBU, R. SUGITA and M. TSUBAKI, *IEEE Trans. Magn.* **MAG-23** (1987) 3654.
105. C. P. G. SCHRAUWEN, J. P. C. BERNARDS, R. W. de BIE, G. J. P. van ENGELEN, H. H. STEL, V. ZIEREN and S. B. LUITJENS, *IEEE Trans. Magn.* **MAG-24** (1988) 1901.
106. O. KITAKAMI, Y. OGAWA, H. FUJIWARA, F. KUGIYA and M. SUZUKI, *IEEE Trans. Magn.* **MAG-24** (1988) 2353.
107. S. HIRONO and A. FURUYA, *IEEE Trans. Magn.* **MAG-24** (1988) 2350.
108. T. TANAKA and H. MASUYA, *Jpn. J. Appl. Phys.* **26** (1987) 897.
109. M. FUTAMOTO, Y. HONDA, H. KAKIBAYASHI and K. YOSHIDA, *IEEE Trans. Magn.* **MAG-21** (1985) 1426.
110. Y. NIIMURA, Y. KITAMOTO, S. NAKAGAWA and M. NAOE, *IEEE Trans. Magn.* **MAG-23** (1987) 2464.
111. E. M. SIMPSON, N. CURLAND and R. T. J. MATZ, *IEEE Trans. Magn.* **MAG-21** (1985) 1450.
112. E. M. SIMPSON and J. H. JUDY, *IEEE Trans. Magn.* **MAG-22** (1986) 1167.
113. W. T. STAM, G. J. GERRITSMA, J. C. LODDER and Th. J. A. POPMA, *IEEE Trans. Magn.* **MAG-23** (1987) 128.
114. M. T. STAM, G. J. GERRITSMA, J. C. LODDER and Th. J. A. POPMA, *IEEE Trans. Magn.* **MAG-24** (1988) 1799.

115. T. TANAKA, E. KANAYAMA, T. KATAHIRA, I. SAITO, K. KAWAZOE and H. MASUYA, *Jpn. J. Appl. Phys.* **27** (1988) 2051.
116. K. KIUCHI, H. WAKAMATSU, F. SUZUKI and H. TAKAGI, *IEEE Trans. Magn.* **MAG-24** (1988) 2341.
117. P. BUTTAFAVA, G. CIARDIELLO and M. PIANO, *IEEE Trans. Magn.* **MAG-20** (1984) 108.
118. F. T. PARKER, *IEEE Trans. Magn.* **MAG-22** (1986) 19.
119. A. KOUCHIYAMA, I. SUMITA, Y. NAKAYAMA and M. ASANUMA, *IEEE Trans. Magn.* **MAG-23** (1987) 2791.
120. A. FUKIZAWA and M. NAOE, *IEEE Trans. Magn.* **MAG-23** (1987) 140.
121. J. P. C. BERNARDS, C. P. G. SCHRAUWEN, Z. ZIEREN and S. B. LUITJENS, *J. Appl. Phys.* **63** (1988) 2897.
122. E. SIMPSON, E. PERSSON, W. BONIN and E. WUORI, *IEEE Trans. Magn.* **MAG-20** (1984) 782.
123. S. B. LUITJENS, C. P. G. SCHRAUWEN, J. P. C. BERNARDS and V. ZIEREN, *IEEE Trans. Magn.* **MAG-21** (1985) 1438.
124. V. ZIEREN, S. B. LUITJENS, C. P. G. SCHRAUWEN, J. P. C. BERNARDS, R. W. de BIE and M. PIENA, *IEEE Trans. Magn.* **MAG-22** (1986) 370.
125. B. BAKER, *J. Appl. Phys.* **55** (1984) 2217.
126. W. T. MALLONEY, *IEEE Trans. Magn.* **MAG-15** (1979) 1546.
127. C. J. ROBINSON, *IEEE Trans. Magn.* **MAG-22** (1986) 328.
128. R. WALMSLEY, J. THOMPSON, D. FRIEDMAN, R. M. WHITE and T. GABALLE, *IEEE Trans. Magn.* **MAG-19** (1983) 1992.
129. Y. NAKAMURA and S.-I. IWASAKI, *IEEE Trans. Magn.* **MAG-20** (1984) 105.
130. S.-I. IWASAKI, *IEEE Trans. Magn.* **MAG-20** (1984) 657.
131. K. OUCHI and S.-I. IWASAKI, *J. Appl. Phys.* **57** (1985) 4013.
132. K. OUCHI and S.-I. IWASAKI, *IEEE Trans. Magn.* **MAG-23** (1987) 2443.
133. T. SUZUKI, *IEEE Trans. Magn.* **MAG-20** (1984) 675.
134. J. C. MALLINSON, *IEEE Trans. Magn.* **MAG-21** (1985) 1217.
135. I. HATAKEYAMA, *Jpn. Annual Review in Electronics, Computers and Telecommunications* **21** (1985/86) 147.
136. Y. NAKAMURA and I. TAGAWA, *IEEE Trans. Magn.* **MAG-24** (1988) 2329.
137. J. HOKKYO, *J. Magn. Soc. Jpn.* **13,** Supplement No. S1 (1989).
138. K. OUCHI, *J. Magn. Soc. Jpn.* **13,** Supplement No. S1 (1989).
139. S. YAMAMOTO, Y. NAKAMURA and S.-I. IWASAKI, Digest of the Fourth Joint MMM-Intermag Conference, EE-02 (1988).
140. K. NAKAMURA and S.-I. IWASAKI, *IEEE Trans. Magn.* **MAG-18** (1982) 1167.
141. S. YAMAMOTO, Y. NAKAMURA and S.-I. IWASAKI, *IEEE Trans. Magn.* **MAG-23** (1987) 2070.
142. J. NUMAZAWA, Y. YONEDA, F. ARUGA and R. HORIUCHI, *IEEE Trans. Magn.* **MAG-23** (1987) 2476.
143. M. DUGAS, M. BONIN and J. JUDY, *IEEE Trans. Magn.* **MAG-23** (1987) 1554.
144. K. NAKAMURA, N. ECHIGO and H. YOHDA, *IEEE Trans. Magn.* **MAG-23** (1987) 2482.
145. J. NUNAZAWA, Y. YONEDA, F. ARUGA and T. HORIUCHI, IEICE Technical Report (in Japanese) MR88-14 (1988).
146. S.-I. IWASAKI and K. OUCHI, *J. Magn. Soc. Jpn.* **13,** Supplement No. S1 (1989).
147. M. SUZUKI, F. KUGIYA, K. YOSHIDA and O. KITAKAMI, *J. Magn. Soc. Jpn.* **13,** Supplement No. S1 (1989).
148. K. OUCHI, *J. Magn. Soc. Jpn.* **13,** Supplement No. S1 (1989).
149. I. T. NUM and Y.-K. HONG, *J. Magn. Soc. Jpn.* **13,** Supplement No. S1 (1989).
150. M. NAOE, M. MATSUOKA and Y. HOSHI, *J. Appl. Phys.* **57** (1985) 4019.
151. K. INOUE, M. YOAHIKIYO and S. YOSHII, *IEEE Trans. Magn.* **MAG-23** (1987) 3651.
152. E. KANAYAMA and H. TAKINO, Digests of the 11th Annual Conference on Magnetism, Japan (1987) 3pA-12.
153. N. WATANABE, Y. ISHIZAKA, K. KIMURA and E. IMAOKA, *IEEE Trans. Magn.* **MAG-21** (1985) 1368.
154. T. TAKAHASHI, T. MIYATA, J. YOSHIDA and T. HATA, *Jpn. J. Appl. Phys.* **24** (1985) L-752.

Received
and accepted 30 April 1990